SURFACE AND INTERFACE ANALYSIS, VOL. 26, 249–269 (1998)

Accuracy of the Non-destructive Surface Nanostructure Quantification Technique Based on Analysis of the XPS or AES Peak Shape

S. Tougaard
Physics Department, Odense University, DK-5230 Odense, Denmark

The accuracy of XPS and AES quantification by peak shape analysis was established from a detailed analysis of a range of model spectra and three sets of experiments. It was found that information on the concentration–depth profile in the surface region up to depths of $\sim 5\lambda_i$ (where λ_i is the inelastic electron mean free path) is primarily contained in the spectral energy region up to ~ 100 eV below the peak energy and is essentially completely contained by the energy region up to ~ 200 eV below the peak. Analysis of a larger energy range than 100 eV does not add much to the information on the details of the structure in the outermost $5\lambda_i$ but gives the possibility to determine additional structural parameters that describe the composition at larger depths. The structural parameters that describe the chemical composition of the outermost $5–10\lambda_i$ of the solid were divided into primary and secondary parameters: the primary parameters are the three most important parameters needed to describe the main characteristics of the distribution of atoms; the secondary parameters are parameters other than the three primary parameters that describe the finer details of the depth distribution of atoms in the outermost $5–10\lambda_i$ of the surface region. The uncertainty in the determined three primary parameters is typically 5–10%. The uncertainty in the determined secondary parameters is typically $\gtrsim 35\%$. Different models of depth profiles can be distinguished when they differ significantly over a width of more than $\sim 1/3\lambda_i$ at any depth $\lesssim 5\lambda_i$. The uncertainty in the total determined amounts of atoms within the surface region is $\sim 5–10\%$ as long as the depths are within the primary probing depth of the method (i.e. $< 5\lambda_i$). The absolute quantification of a set of samples where the in-depth distribution varies considerably gives a root-mean-square scatter of 15%. This is reduced to $\sim 10\%$ when elastic scattering effects are modelled by a simple analytical expression. © **1998 John Wiley & Sons, Ltd.**

Surf. Interface Anal. **26**, 249–269 (1998)

KEYWORDS: quantitative surface analysis; XPS; AES; nano-structures; peak shape analysis

INTRODUCTION

In the past 30 years there has been a continuous effort to improve the accuracy of x-ray photoelectron spectroscopy and Auger electron spectroscopy (XPS and AES).[1–14] The motivation for this is the high and continuously growing technological importance in this time period of the properties of solid surfaces on the nanometre depth scale. Algorithms for quantification rely on several factors, such as reliable values of the inelastic electron mean free path (λ_i), good descriptions of elastic scattering effects and accurate procedures to determine the analyser transmission as a function of energy. To secure a cost-effective output from this effort, it is important to stress the obvious fact that when several factors contribute roughly equally to the error, even a considerable improvement in the uncertainty from a single factor has essentially no influence on the total error. When we want, in the future, to improve procedures for quantitative surface analysis by XPS and AES, it is then necessary first to establish those leading factors that contribute most to the error. It is these factors that should be the focus of research, because if their accuracy is not improved, any improvement in the less important factors will have essentially no influence on the accuracy of the quantification procedure. In a previous paper[14] we compared the errors associated with different factors. It was shown that the factor that by far contributes most to the inaccuracy in quantification is the lack of knowledge of the in-depth composition of the solid. For a meaningful quantification, assumptions on the in-depth distribution of atoms must be made because the measured peak intensity depends strongly on this. In practical analysis, however, the in-depth atomic distribution is never known, because if it were it would be a waste of time and effort to do the analysis. Usually the solid composition is, for convenience, quite arbitrarily assumed to be homogeneous up to a depth of several nanometres and then the surface concentration will be proportional to the measured peak intensity. This assumption may result in enormous errors in quantification.[9,14] Thus, the in-depth composition of solids that are analysed by XPS and AES is hardly ever known to be homogeneous up to a depth of several nanometres. It is precisely because samples are *inhomogeneous* on the nanometre depth scale that analysis is done with XPS or AES, rather than with other well-established[15] but less surface-sensitive techniques.

To illustrate the fundamental problem with the assumption of homogeneous composition with depth, we consider an example of model spectra calculated for

* Correspondence to: S. Tougaard, Physics Department, Odense University, DK-5230, Odense, Denmark.

CCC 0142–2421/98/040249–21 $17.50

Received 19 September 1997
Accepted 3 December 1997

different depth distributions. Thus, Fig. 1 shows spectra of the Cu 2p peaks corresponding to four different surface morphologies.[14] The XPS peak intensity from all four solids is exactly identical, although the surface compositions are widely different. Analysis of these spectra under the assumption that the surface concentration is proportional to the peak intensity would result in a quantification where the inaccuracy is such that the true concentration at the surface could be anywhere from 0% [as in (d)] to 100% [as in (a)] and the true total amount of copper material within the surface region could be anywhere from the equivalent of 1.1 Å [as in (a)] or 10 Å [as in (c)] or even higher [as in (d)]. The uncertainty in quantification is consequently several hundred per cent. Quantification based on peak intensities alone is thus subject to incredibly large uncertainties.

From the above, the clear conclusion is that our focus of research should be to improve spectral analysis of XPS and AES such that it provides information on the in-depth distribution of atoms on the nanometre depth scale. Without this, we can expect essentially no improvements in the accuracy of XPS and AES even if we find substantially better descriptions of other parameters in the quantification procedure.

From Fig. 1, it is clear that the peak shape in a wider energy range below the peak depends critically on the in-depth distribution of the element. It would thus be very easy to distinguish experimentally between the peak shape of the four spectra in a 100 eV energy region. Much more accurate quantification can therefore be achieved if the dependence of peak shape on surface morphology is taken into account in the analysis. This is the idea behind the formalism developed by Tougaard *et al.*,[7–9,14,16–18] which provides quantitative information on the surface nanostructure of the solid by analysis of XPS or AES peak shapes. The technique relies on the phenomenon seen in Fig. 1: that the energy loss structure that accompanies an XPS or AES peak carries information on the depth of origin of the detected electrons. The method is non-destructive and therefore allows the change in surface morphology if a given surface atomic structure during surface treatment (e.g. chemical reactions and gradual annealing) to be studied. It has been applied in the study of a wide range of systems and physical phenomena,[19–41] including growth mechanisms and nanostructures of metal/metal,[20,28] silicon/metal,[32–34] silicon/germanium[41] and polymer/metal systems,[29,31] carbon segregation on Ni,[35] metal oxide growth[19] and the depth excitation function in electron-stimulated AES.[38–40] Several tests on the validity of the method have also been done.

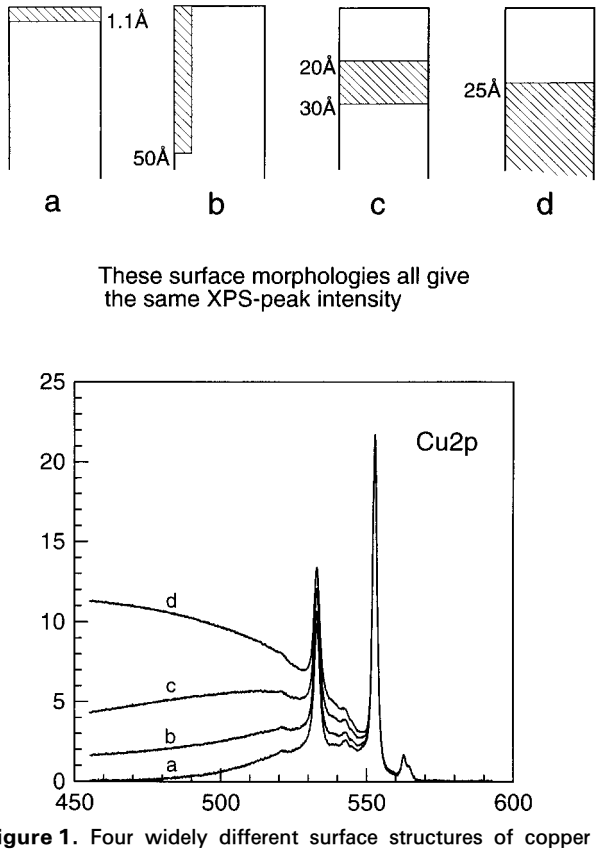

Figure 1. Four widely different surface structures of copper in gold that give identical peak intensities.

It is the purpose of the present paper to give a critical evaluation of the potential of this technique. We will determine the accuracy of quantification and also the accuracy with which the technique can determine details of the in-depth distribution of atoms on the nanometre scale.

THEORY

To obtain a practical and useful model, we treat electron excitation and electron transport as separate events. It is well known that this assumption is not strictly valid,[42–46] but at typical XPS and AES energies it is valid to a good approximation, as we will now argue. It was shown many years ago that at low energies, where the outgoing photoelectron or Auger electron has an energy of a few times the plasmon energy, the plasmon intensity is diminished considerably due to a quantum interference term between the extrinsic and the intrinsic plasmon excitations.[42–45] The effect may be significant when the energy of the excited electron is only a few times the typical energy loss in a single scattering event. The most probable energy loss for electrons moving in solids is, in general, $\sim$10–30 eV.[47,48] In ultraviolet photoelectron spectroscopy (UPS) where the energy of the outgoing electron is typically <50 eV, the interference terms are therefore important and it is then a questionable approximation to evaluate such energy spectra within a model where the excitation and transport processes are treated as separate effects. The quantum interference term becomes less important at high energies because the intrinsic and extrinsic plasmon excitations become decoupled by mainly occurring in spatially separated regions. For the spectroscopies of interest here, where the typical electron energy exceeds 200 eV, the interference term is therefore of minor importance and it is a reasonable approximation to treat the processes as separate effects and divide the effects into an excitation process, which includes any intrinsic excitations (see below), and a transport process where changes in peak shape result from electron scattering during transport to the surface.

The peak shape of a photon-excited core level is inherently Lorentzian, the width of which is the inverse of the core-hole lifetime. Photon broadening with essentially a Gaussian character will, particularly for polar

materials, add considerably to the line width determined by lifetime broadening in both XPS and AES.[42] Measured peak shapes will generally be mixed, with additional Gaussian broadening originating from the response function of the spectrometer. The photoelectron peak shape is also greatly influenced by what is known as the many-body phenomenon,[42–45,49–52] which results in so-called intrinsic excitations: after the core electron has been photon excited, the potential from the resulting core hole leads to electron–hole pair excitations near the Fermi level[50] and to plasmon excitations of the valence sea of electrons.[51,52] For metals, where the density of electron states (DOS) is high in the region of the Fermi level, the former process leads to a skewed peak shape toward lower binding energy and the effect in the immediate vicinity of the peak is larger for solids with a large DOS at or near the Fermi energy. For energies of only a few electron-volts from the peak energy, where the valence band DOS may be considered roughly constant, the combined effect of these electron–hole pair excitations and the lifetime broadening is described by a formula due to Doniach and Sunjic.[49] This formula is, however, not a valid approximation for the full extension of the intrinsic peak. In fact, the Doniach–Sunjic formula fits the experimentally observed XPS peak shapes in an energy range of only a couple of electron-volts from the peak energy. More than a few electron-volts from the peak energy, the structure in the DOS and the contribution from intrinsic plasmon excitations[51,52] will cause the excitation probability of the various electron–hole pair processes to vary with energy and the intrinsic peak shape deviates considerably from the simple Doniach–Sunjic form.[52]

In the energy region around 10–30 eV below the peak energy, corresponding to the region of plasmon excitations, intrinsic excitations have been found to account for about one-third of the measured intensity in XPS peaks from both simple metals[51] and transition metals.[52] These findings have recently been confirmed directly by Auger photoelectron coincidence spectroscopy.[53] The intrinsic excitations then cause XPS peaks to extend typically ~ 50 eV below the peak energy.[52]

During transport out of the solid, the electrons experience inelastic scattering events. This leads to a distortion of the energy distribution compared with the original distribution at the point of excitation in the solid. It is thus the inelastic scattering processes that are responsible for the transport-induced changes in peak shape. However, elastic scattering[6] as well as diffraction and forward focusing effects[54,55] also occur and these will indirectly influence the peak shape. The energetic electrons are emitted from the atom with an angular distribution determined by the excitation process. Elastic scattering leads to a change in the angular distribution of electrons and will also cause the electron trajectories to deviate from straight lines. The measured energy spectrum will then have contributions from electrons that have followed different paths with a relative weight determined by the elastic scattering cross-section. It turns out that for energies of interest in XPS and AES (i.e. $\gtrsim 100$ eV), small-angle scattering is far most probable[56] and this tends to favour trajectories where most of the emitted electrons have followed nearly straight lines.

In the next section we briefly discuss models to describe the measured peak shapes and then we go on to discuss models that describe the connection between atomic in-depth composition profile and peak shape.

Photoelectron peak shapes

After the photoexcitation process, some of the electrons are transported to the surface and enter the spectrometer. Quantification relies on an accurate description of how this transport influences the energy spectrum. For inhomogeneous samples, the effect is substantial (see Fig. 1) and quantification requires a detailed and accurate description of inelastic electron scattering. The total energy loss of an electron moving in a solid is determined by the inelastic scattering cross-section. Multiple scattering events are important, because in typical cases the energy spectrum includes electrons that have travelled a distance of several inelastic electron mean free paths.

Let $F(E_0, \Omega_0, x)\mathrm{d}^2\Omega_0\,\mathrm{d}E_0\,\mathrm{d}x$ be the flux of electrons excited at depth x, $\mathrm{d}x$ in an energy interval E_0, $\mathrm{d}E_0$ into the solid angle Ω_0, $\mathrm{d}\Omega_0$ and let $Q(E_0, \Omega_0, x; R, \Omega)\mathrm{d}R\,\mathrm{d}^2\Omega$ be the probability that an electron excited with energy E_0 at depth x in direction Ω_0 will arrive at the surface in the direction Ω, $\mathrm{d}^2\Omega$ after having travelled the path length R, $\mathrm{d}R$. Then the number of electrons emitted per second, per unit energy and solid angle is[7]

$$J(E, \Omega) = \int \mathrm{d}E_0 \int \mathrm{d}^2\Omega_0 \int \mathrm{d}x\, F(E_0, \Omega_0, x) \times \int Q(E_0, \Omega_0, x; R, \Omega) G(E_0, R; E)\mathrm{d}R \quad (1)$$

where $G(E_0, R; E)\mathrm{d}E$ is the probability that an electron with initial energy E_0 has energy in the interval E, $E + \mathrm{d}E$ after having travelled the path length R.

It is possible in principle that the energy distribution at the point of excitation may vary with depth. This may arise as a result of peak shape dependence on the local chemical composition, which in a typical sample will vary with depth. This effect may also occur even in a homogeneous solid, because the difference in the chemical environment of an atom present in the surface layer to that of an atom situated a few layers underneath the surface may lead to differences in electron energy levels and in the local density of electron states (DOS). This in turn will affect the response of the surrounding electrons to the excitation process and thus affect also the shake-up processes and consequently the energy distribution of emitted electrons. Because these depth-dependent effects are usually small and a complete quantitative description is not practically possible because of lack of detailed models of general validity, it is usually a valid and reasonable approximation to assume that the concentration of electron emitters $f(x)$ may vary with depth x but that the energy distribution is independent of depth, i.e.

$$F(E_0, \Omega_0, x) = f(x)F(E_0, \Omega_0) \quad (2)$$

where $F(E_0, \Omega_0)\mathrm{d}^2\Omega_0\,\mathrm{d}E_0$ is the number of electrons per second, per atom and per unit energy excited in an energy interval E_0, $\mathrm{d}E_0$ into the solid angle Ω_0, $\mathrm{d}^2\Omega_0$ and $f(x)$ is the number of atoms per unit volume at depth x.

Elastic electron scattering, which we discuss in the following section, enters as a path-length-increasing effect and is described by the function Q in Eqn (1).

Elastic electron scattering. The inelastic processes are clearly the dominating factor in interpretation of measured peak intensities and peak shapes. Quantification therefore relies on accurate values for the inelastic scattering cross-section and the inelastic electron mean free path λ_i.

In this section we will discuss some effects of elastic electron scattering in quantitative interpretation of XPS. Elastic scattering effects have often been neglected in practical applications of the peak shape analysis method. We will therefore discuss the validity of this approximation first. In a recent systematic study of Monte Carlo-simulated peak intensities[57] it was found that for typical geometries applied in practical XPS analysis the influence of elastic scattering is small and amounts to $\lesssim$10–15% for electrons from depths $\lesssim 1.5\lambda_i$, while for electrons emitted at larger depths, the elastic electron scattering gives a substantial reduction in the measured peak intensity.

The effect of elastic electron scattering on quantitative XPS of homogeneous solids, where most of the peak intensity comes from depths $\lesssim\lambda_i$, will consequently also be small. This was studied for a particular XPS geometry in Ref. 58, where intensity ratios of experimental XPS peaks from several one-element solids were compared to two first-principle theories corresponding to neglecting and including the effects of elastic electron scattering. Elastic electron scattering was simulated by a Monte Carlo calculation. The theoretical peak intensities were found to change by an average of 14% as a result of elastic scattering. Surprisingly, however, the standard deviation between theory and experiment was practically unchanged, namely $\sim$15% in both cases (i.e. whether neglecting or including elastic scattering effects). This points to the conclusion that for practical analysis of homogeneous solids it makes only a very small improvement in the accuracy of quantification to include elastic scattering effects.

This result can be understood from the following consideration. The error on quantification for the peaks from the pure elemental solids depends mainly on the accuracy of six factors: the ratio of inelastic mean free paths, the ratio of photoionization cross-sections, the procedure for peak intensity determination (i.e. the method used for inelastic background correction), the influence of elastic electron scattering, the stability of the instrument and the energy dependence of the electron spectrometer transmission function. (Other factors will also contribute to the error, such as the role of surface roughness and surface plasmon excitations, but for simplicity we assume that the error comes from the above-mentioned six factors.) Let us assume that all factors contribute with the same amount to the error and let us assume that this is 6% for each factor (this number is chosen just to illustrate a point and is quite arbitrary but probably not too far from reality). The total relative error due to these six factors is 14.7% which is close to what was observed in the comparison of XPS peak intensity ratios to theory[58] (see above). Let us then assume that, somehow, we are able to completely eliminate the uncertainty from one of these six factors. Then we have five factors each contributing 6% to the error and this results in a relative error of 13.4%. This is only slightly smaller than 14.7% and illustrates that when several factors contribute roughly equally to the error, even a considerable improvement in the uncertainty from a single factor has only little influence on the total error.

Different analytical formulae to describe the effects of elastic electron scattering have been proposed in the past.[59–63] As the example discussed above shows, the effects of elastic electron scattering are often small. It therefore seems natural to treat them by a correction factor to a calculation where elastic scattering effects have been neglected. This was done recently by Jablonski and Tougaard,[63] and they found a simple yet rather accurate formula valid for typical geometries applied in practical XPS and AES. They formulated the effect of elastic scattering on peak intensity as a simple correction factor (CF) to the result of a description that neglects elastic scattering. The CF is the ratio of emitted peak intensity from a layer of atoms located at a given depth z in a solid calculated from theories that take into account (I^{el}) and neglect (I^{nel}) elastic electron scattering. They made extensive Monte Carlo calculations of CF under variation of the full relevant parameter range of electron energy, matrix atomic number, depth x of origin of emitted electrons and angular emission anisotropy. By expressing these results in units of the dimensionless variable x/λ_{et} they found the following general analytical expression[63]

$$CF(x/\lambda_{et}) = I^{el}/I^{nel} = \exp[-0.1578(x/\lambda_{et}) - 1.251] + \exp[-0.05624(x/\lambda_{et})^2 + 0.006988(x/\lambda_{et}) - 0.2020] \quad (3)$$

where $\lambda_{et} = (\lambda_i \lambda_{tr})/(\lambda_i + \lambda_{tr})$ and λ_{tr} is the transport mean free path for elastic electron scattering. Three assumptions were made in the calculations, namely that the geometry is close to normal emission, that the angle between x-ray source and analyser axis is close to the magic angle (54°) and that the ratio λ_{tr}/λ_i is approximately constant over the analysed depth. However, the result deviates only slightly from Eqn (3) when these assumptions are not strictly fulfilled.[64] Equation (3) provides a very simple way to correct peak intensities for elastic scattering effects. Let the in-depth concentration profile be given by the function $f(x)$ describing the number of atoms per unit volume at depth x. When elastic scattering is neglected, the measured peak intensity from this solid is

$$I^{nel} = I_0 \int_0^\infty f(x)\exp\left(-\frac{x}{\lambda_i \cos\theta}\right)dx \quad (4)$$

where θ is the emission angle with respect to the surface normal and $I_0 \lambda_i \cos\theta$ is the intensity from a solid with $f(x) \equiv 1$. The measured intensity when elastic scattering is accounted for is

$$I^{el} = I_0 \int_0^\infty CF(x/\lambda_{et}) f(x)\exp\left(-\frac{x}{\lambda_i \cos\theta}\right)dx \quad (4a)$$

where we have assumed that λ_{et} is approximately constant in the surface region. When λ_{et} varies considerably over the analysed depth, Eqn (4a) is no longer strictly valid.

It was shown in Ref. 64 that the general expression for the function *CF* [Eqn (3)] is to a good approximation valid for depths up to 50 Å when the angle between axis of the analyser and the x-rays is in the range 45–65°, the emission angle is $<30°$ and the transport mean free path λ_{tr} is in the range $1.3\lambda_i \leqslant \lambda_{tr} \leqslant 7\lambda_i$. The latter condition is satisfied for essentially all XPS peaks. For depths $\leqslant 2\lambda_{et}$, the root-mean-square (RMS) deviation between *CF* [Eqn (3)] and the ratios calculated by Monte Carlo simulations amounts to $\sim 5\%$.[64]

Except where explicitly mentioned, in the calculations presented in this paper we will neglect elastic electron scattering. Because of elastic electron scattering, the depth of origin is different from the path length travelled by the electron. The importance of this effect can be estimated from the results of Ref. 63. From figure 4 of that paper, the path-length-increasing effect of elastic scattering is small for depths smaller than $\sim 1.5\lambda_i$. For larger depths the effect increases, and for depths of ~ 3–$5\lambda_i$ the intensity is seen (Fig. 4 of Ref. 63) to be decreased by an additional factor of ~ 3 due to elastic scattering effects. A decrease in intensity of a factor of 3 corresponds to a path length increase of $\sim 1\lambda_i$. An electron excited at depth $\sim 4\lambda_i$ has consequently moved an average distance of $\sim 5\lambda_i$ before being emitted. As a rough estimate, the actual distance that emitted electrons have travelled in the solid is thus, on average, ~ 15–30% larger than the straight-line distance from the point of excitation to the surface.

Forward focusing and diffraction effects. Because elastic scattering of electrons on atoms is much more probable in the forward direction,[56] structures in measured spectra as a function of emission angle are frequently observed with maxima occurring in directions corresponding to emitted electrons being scattered on neighbouring atoms.[54,55] Variations as high as 30–50% in measured peak intensities as a function of take-off angle have been observed.[54,55] The enhanced intensity is caused by focusing in the forward direction of the emitted electrons by the attractive Coulomb potential on neighbouring atoms. In a simple qualitative picture, this leads to enhanced intensity in directions that directly correspond to the near neighbours of the electron-emitting atom. In XPS of Al(001)[65] and of NiO, MnO and CoO,[66] this forward-focusing effect was investigated in the peak energy region as well as in the energy loss region below the peak energy. By observing the intensity variation as a function of both the emission angle and the energy distance to the peak, it was found that the further the energy distance to the main peak, the less structure is observed in the measured intensity. This was interpreted as being due to a substantial reduction in the forward focusing for the electrons that originate from deeper layers. Thus, electrons below a peak energy have travelled a typical distance roughly in proportion to their energy loss. The mean energy lost per inelastic mean free path travelled is ~ 15–30 eV.[47,48] Features due to forward focusing observed experimentally are then concluded to originate predominantly from electron emitters within the outermost two to four layers of atoms.[55] Several examples of the forward-focusing effect have been reported.[54,55,65–68] To account quantitatively for the effect as well as the finer details in the intensity variations with take-off angle, detailed models are being used with considerable success.[54,55,67] Analysis of the preferred angular directions of Auger or photoelectrons therefore gives very direct information on the geometric arrangement of the outermost atoms and has led to the development of a powerful technique for investigations of the atomic surface structure.[54,55]

Although an advantage for investigations of the geometrical structure of surface atoms, forward-focusing effects have severe negative implications for quantitative surface composition analysis by AES and XPS of single-crystalline substrates. It can lead to errors as high as 50% in determined stoichiometries.[54,55,65,66] Averaging over several directions will reduce the effect.[54,66,69] This is, however, often impractical because the total data collection time is severely increased or it may even be impossible because many instruments do not allow for variations of both azimuthal and polar angles of the electron energy analyser. The effects are largely avoided in polycrystalline and amorphous materials as long as the polycrystalline material is free of preferential crystal orientation.[69] In any case, ion bombardment used for sample cleaning, for example, will to some extent destroy the crystal structure in the outermost two to four atomic layers and will thus tend to reduce forward-focusing and diffractions effects.

Inelastic electron scattering. The detailed energy distribution G of electrons as a function of the path length travelled in the solid can be calculated provided that the energy loss probability per unit path length travelled is known. If elastic scattering effects are neglected, the energy spectrum of emitted electrons is

$$J(E, \Omega) = \int \mathrm{d}E_0\, F(E_0, \Omega) \int f(x) G(E_0, x/\cos\theta; E)\mathrm{d}x \tag{5}$$

where θ is the emission angle with respect to the surface normal. The function G, which essentially gives the energy distribution of an electron as a function of path length $x/\cos\theta$ travelled in the solid, is thus of central importance in any quantitative analysis of energy spectra of emitted electrons. It is determined by the inelastic scattering cross-section.

We denote by $K(E, T)$ the differential inelastic scattering cross-section, i.e. $K(E, T)\mathrm{d}R\,\mathrm{d}T$ is the probability that an electron of energy E will lose energy in the interval T, $T + \mathrm{d}T$ after having travelled a path length $\mathrm{d}R$ in the solid. In general $K(E, T)$ depends strongly on T, moderately on the specific solid and only weakly on E.[47,48] For energy spectra where the total energy loss is small compared with the primary electron energy, $K(E, T) \cong K(T)$, i.e. independent of E. Then the effect of multiple scattering has a rigorous solution and the spectrum of emitted electrons is

$$J(E, \Omega) = \int \mathrm{d}E_0\, F(E_0, \Omega) \int \mathrm{d}s\, \mathrm{e}^{-i2\pi s(E-E_0)} \times \int \mathrm{d}x\, f(x)\, \mathrm{e}^{-x\Sigma(s)/\cos\theta} \tag{6}$$

with

$$\Sigma(s) = \frac{1}{\lambda_i} - \int_0^\infty K(T)\, \mathrm{e}^{-isT}\,\mathrm{d}T \tag{7}$$

Inelastic electron scattering is clearly the dominating first-order effect in quantitative understanding of peak intensities and peak shapes, and this has been the subject of several papers.[19–41]

Inelastic electron scattering cross-section. For practical application of the above formalism, it is essential to have methods for fast calculations of the energy loss of electrons at any energy as they move in solids of general and non-uniform composition. This is possible with the Universal cross-section that was introduced a decade ago.[47] Recently, a critical review of the Universal cross-section was given[48] in the light of the results of research carried out since it was first introduced. In particular, its validity was compared to the validity of experimental cross-sections determined by analysis of reflected electron energy-loss spectra (REELS). It was shown that for applications in quantitative surface analysis by XPS and AES, the solids can be divided into classes according to the full width at half-maximum of the dominating shape of the inelastic scattering cross-section. Depending on the class of materials, a function with either two or three parameters is needed to describe the most important general characteristics common to the cross-sections of that class.[48]

For most metals, their oxides and alloys, the *Universal cross-section*[47,48]

$$\lambda_i(E)K(E, T) = \frac{BT}{(C + T^2)^2} \tag{8}$$

with $C = 1643$ eV^2 and $B \approx 3000$ eV^2 applies with reasonable accuracy. The cross-section is normalized to unit area for $B = 2C = 3286$ eV^2. This cross-section was successfully applied in studies of many systems (including pure metals, alloys, metal oxides and thin films of metals and metal oxides).

For solids with a narrow plasmon structure, the cross-sections cannot be well described by a function with two parameters. For these, however, it was shown[48] that the main characteristics of the cross-section can be described by the *Three-parameter Universal cross-section*

$$\lambda(E)K(E, T) = \frac{BT}{(C - T^2)^2 + DT^2} \tag{9}$$

where the three parameters B, C and D have been determined for each class of materials (e.g. polymers, semiconductors, free-electron-like solids[48]).

It was shown[48] that the Universal cross-section (Eqn (8)) is quite accurate for solids when their cross-section has a width at half-maximum $\gtrsim 20$ eV. For solids with a cross-section width of 10–15 eV, the Universal cross-section is still fairly good for the description of the far peak region ($\gtrsim 30$ eV from the peak energy) but it is less accurate to account for the near peak region ($\lesssim 10$ eV from the peak energy). For the solids with a cross-section width $\lesssim 5$ eV, the Three-parameter Universal cross-section [Eqn (9)] is always more accurate than the Universal cross-section.

Quantitative XPS by peak shape analysis

There are two different approaches to the application of the new formalism: either algorithms are used to remove the inelastic background from the measured spectrum; or the peak shape of the spectrum of emitted electrons is calculated. In both cases spectral evaluation is done by formulae that depend on the in-depth concentration profile $f(x)$.

The ideas for improved quantification briefly described below have been made available in the form of a software package QUASES™ (Quantitative Analysis of Surfaces by Electron Spectroscopy),[18] which was used in all spectral analysis in the present work.

Quantification by peak shape calculation. In this approach, the spectrum $J(E, \Omega)$ is calculated by Eqn (6). The function $F(E, \Omega)$ may conveniently be determined by the procedure described in the next section from a measured spectrum of a pure elemental sample. The in-depth concentration profile $f(x)$ is then varied until a good agreement with the measured spectrum is obtained. In this way, the detailed in-depth concentration profile $f(x)$ is determined.

Quantification by background removal. Formulae to determine the atomic excitation function $F(E, \Omega)$ from a measured spectrum were developed for different types of in-depth profiles.[7–9,14,16–18] It was shown that the integral equation [Eqn (6)] may be solved rigorously for the primary excitation spectrum $F(E, \Omega)$.

$$F(E, \Omega) = \frac{1}{P_1}\left\{J(E, \Omega) - \int dE'\, J(E, \Omega) \int ds \times \exp[i2\pi s(E' - E)]\left(1 - \frac{P_1}{P(s)}\right)\right\} \tag{10}$$

where

$$P(s) = \int dx\, f(x)\exp\left[-\frac{x}{\cos\theta}\,\Sigma(s)\right] \tag{11}$$

and

$$P_1 = \int dx\, f(x)\exp\left(-\frac{x}{\lambda_i \cos\theta}\right) \tag{12}$$

Equation (10) may be used to determine either $F(E, \Omega)$ if $f(x)$ is known (e.g. for a one-element sample) or to determine $f(x)$ if $F(E, \Omega)$ is known. The exact peak shape in the energy region close to the peak energy up to ~ 20 eV below the peak energy is not known because it is largely determined by the chemical bond, lifetime broadening and intrinsic excitations in the photoemission process, all of which may depend on the local chemical environment. However, the spectrum after background correction must be of zero intensity in an energy region beyond ~ 30 eV below the primary peak energy. Furthermore, it was pointed out that the spectral intensity must stay at zero intensity for all energies below the peak energy until the energy of another peak in the energy spectrum is reached. This puts a strong constraint on the function $F(E, \Omega)$ and this may be applied as a criterion to determine $f(x)$ in the sense that $f(x)$ is varied until the constraint is fulfilled. As another criterion, one can use knowledge on $F(E, \Omega)$ determined from the analysis of spectra from samples with a well-characterized in-depth concentration profile, such as a single-element solid. One should be aware of the possible peak shape changes caused by the difference in

chemical environment of the atoms in the reference sample and the sample being investigated. To the extent that these differences can be neglected, the spectrum may be applied as a reference and $f(x)$ is varied until analysis yields a spectrum with the same absolute intensity and peak shape as the reference spectrum. If the peak shape analysis includes peaks from all the elements in a sample, then the constraint that the sum of the concentration of the individual elements at any depth must add up to 100% may also be applied.

OBJECTIVES OF QUANTIFICATION

The main purpose of this paper is to study the accuracy of quantification with XPS and AES based on the present knowledge about the physics behind the techniques. To do this, we must first define the objectives of XPS and AES quantification. This is necessary because the accuracy depends on what one attempts to quantify. For example, XPS may give detailed and rather accurate information on the composition of the outermost few atomic layers but the quantification of depths more than say 100 atomic layers is naturally subject to a much larger uncertainty. Likewise, parameters that describe the approximate depth distribution of atoms in the surface region can be quantified with much better precision than parameters that describe the finer detail of in-depth distribution. The question of accuracy of quantification is therefore not well defined unless we divide it into several more specific questions. This division must be based on a study of the physical processes because it is these that will determine the accuracy. This is done here.

There is a strong correlation between the intensity of a given spectral energy region and the depth where these electrons were emitted. As an example, the peak intensity depends strongly on the atomic concentration at depths $\lesssim 1\lambda_i$ but is rather independent of the concentration at depths exceeding $3\lambda_i$ below the surface. On the other hand, the spectral intensity 100 eV below the peak energy depends strongly on electrons excited at depths of $3–4\lambda_i$ but depends less on the concentration for depths $\lesssim 1\lambda_i$. Different energy regions of the spectrum thus carry information on the atomic concentration at different depths. We must therefore divide the surface region into different regions of depth and, likewise, we must also divide the spectrum into different energy regions below the peak energy. This division will be made in the next section.

Having determined the connection between depths and spectral energy regions we will then go on to determine how much information about the detailed concentration–depth profile can be determined with reasonable accuracy. As we shall see, the certainty with which a given structural parameter is determined depends on the number of parameters that are used to describe the details of the depth profile. Thus, if we consider only a few parameters that describe the rough structure of the sample, the uncertainty on each parameter is smaller than the uncertainty if we use more parameters in an attempt to determine more details of the chemical structure of the surface region. We will divide the structural parameters into primary and secondary parameters: primary parameters define the rough nanostructure of the depth composition; secondary parameters define the finer details of the depth composition. As expected, we will find that the uncertainty of the primary structural parameters is smaller than that of the secondary parameters.

Depth of origin of electrons in a spectrum

Different energy regions of a spectrum have intensity contributions that originate from electrons excited at different depths. In this section we estimate the depth of origin of electrons that contribute to the various energy regions of a spectrum. This knowledge is then used to divide the solid into two regions of depths. Before we consider detailed quantitative model calculations, we will first make a rough estimate based on a simple model.

Let us denote the typical energy loss in a single scattering event by δE. Then the intensity in an energy range ΔE below the peak energy is primarily determined by the distribution of electron emitters within the outermost depth range

$$R = \frac{\Delta E}{\delta E} \times \lambda_i \tag{13}$$

ΔE is typically $\sim$15–30 eV depending on the solid.[47,48] As an example, $\Delta E = 100$ eV yields $R \sim 4–7\lambda_i$. The spectrum in an energy range up to $\sim$100 eV from the peak energy is then primarily determined by the composition within the outermost $5\lambda_i$. The contribution from electrons excited at larger depth will be small.

We will now consider detailed model calculations of spectra for different in-depth distributions of electron emitters and use these results to establish the connection between path length travelled and the energy region of the spectrum. The model spectra are calculated (with an existing software package[18]) for electron emission normal to the surface and using the normalized Universal cross-section (i.e. $B = 2C = 3286$ eV^2).[48] The correlation between energy loss and depth will scale with the inelastic electron mean free path λ_i. All depths are therefore given in units of λ_i.

The aim is to find the correlation between the depth of origin of emitted electrons and their energy loss ΔE, i.e. their energy ΔE below the peak energy in the measured spectrum of emitted electrons. To this end we define two measures for the connection between spectral intensity contribution and depth of excitation.

For the *first measure* we take a thin layer of material, place it at varying depths z below a surface and monitor the intensity in the emitted spectrum at energy ΔE below the peak. We define three depths: $z0$ is the depth where the layer gives the highest contribution to the intensity and $z1$ and $z2$ are the two depths where the same layer gives half of that intensity contribution.

Figure 2 shows spectra of a 1 Å thick layer of atoms placed in gold at the three depths $z0$, $z1$ and $z2$ valid for $\Delta E = 100$ eV [Fig. 2(a)] and $\Delta E = 200$ eV [Fig. 2(b)]. The values determined for $z0$, $z1$ and $z2$ are plotted in Fig. 4 for energies ΔE up to 500 eV below the peak energy. It is seen that the contribution to the spectral intensity at a given energy comes from a range of depths. For example, at 100 eV below the peak energy

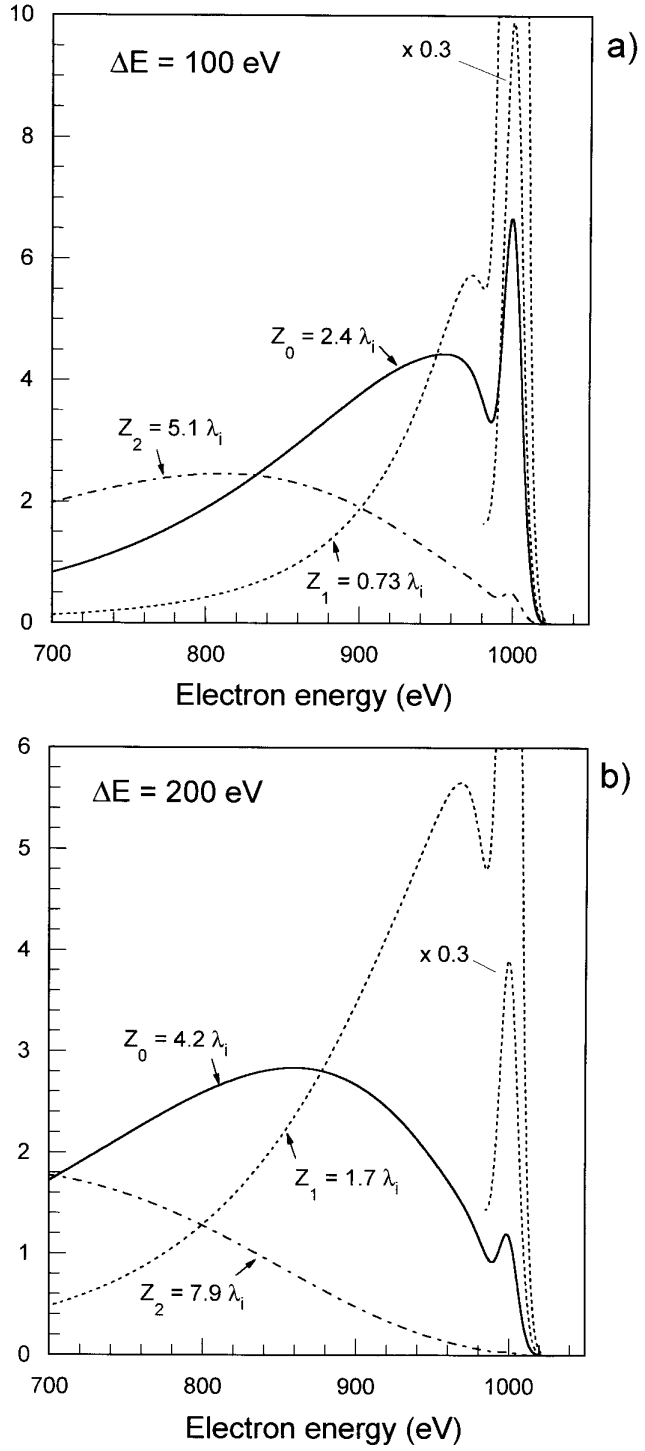

Figure 2. Model spectra from a 1 Å thick layer of material that emits electrons of 1000 eV energy. The layer is placed at varying depths z below a surface: $z0$ is the depth where the layer gives the highest contribution to the intensity ΔE below the peak energy; $z1$ and $z2$ are the two depths where the same layer gives half of that intensity contribution. The solid has inelastic mean free path λ_i and the Universal inelastic scattering cross-section [Eqn (8)].

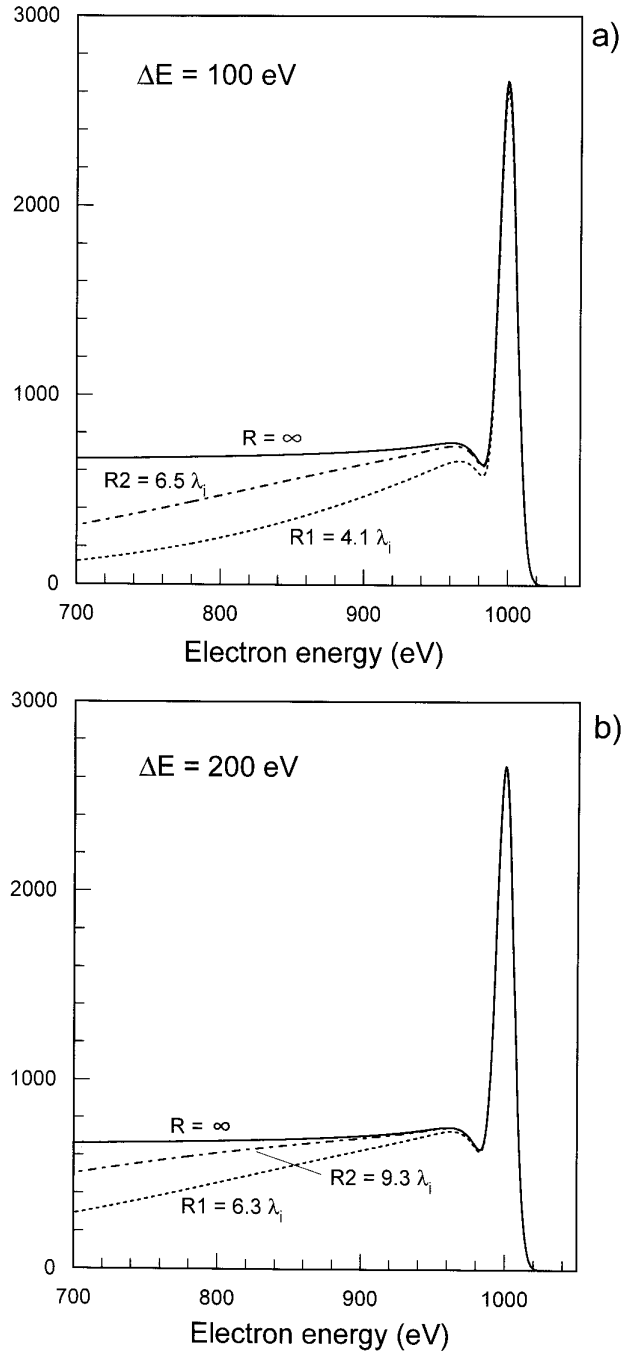

Figure 3. Model spectra from a solid with constant concentration that extends from the surface to the depth R: $R1$ and $R2$ are the values for R for which the intensity ΔE below the peak energy is respectively 67% and 90% of the intensity from a homogeneous solid ($R = \infty$). The solid has inelastic mean free path λ_i and the Universal inelastic scattering cross-section [Eqn (8)].

the spectral intensity contribution from electrons that are excited at all depths between $0.73\lambda_i$ and $5.1\lambda_i$ varies by only a factor of two.

For the *second measure* we take a solid with constant atomic concentration extending from the surface down to depth R. When R is infinity we have a homogeneous solid. We monitor the intensity in the emitted electron spectrum at energy ΔE below the peak. For a given energy ΔE we now find the values $R1$ and $R2$ of R for which we get respectively 67% and 90% of the intensity that we get from a homogeneous solid. Figure 3 shows spectra for $\Delta E = 100$ eV and $\Delta E = 200$ eV. The values of $R1$ and $R2$ are plotted in Fig. 4 as a function of ΔE.

From Figs 2–4, and from further extensive investigations not presented here, we conclude that the intensity and shape of the spectrum in the energy range up to ~100 eV from the peak are primarily determined by the concentration of electron emitters within the outermost

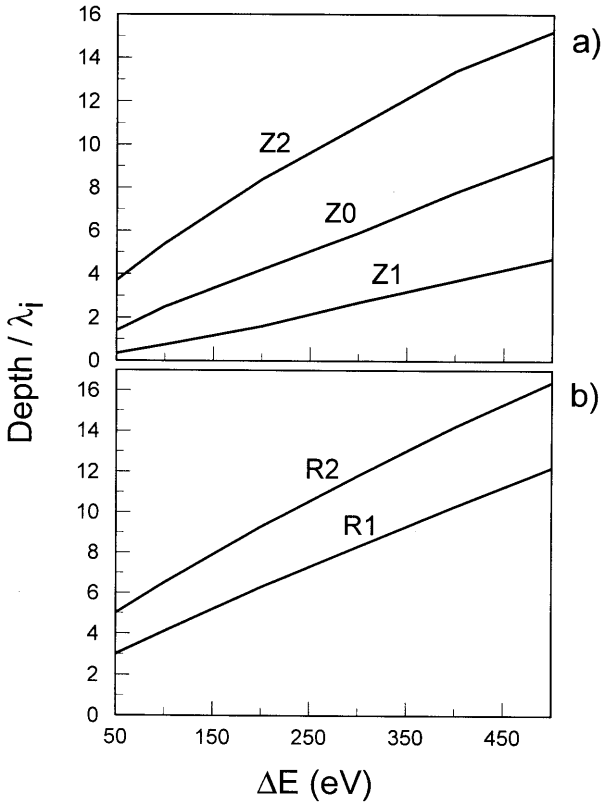

Figure 4. Values of $z0$, $z1$, $z2$, $R1$ and $R2$ in units of λ_i as a function of ΔE.

$5\lambda_i$ and are essentially completely determined by the electron emitters within $8\lambda_i$. For $\Delta E > 100$ eV, the corresponding depths are larger (see Fig. 4). For example, it was previously found that information on the depth excitation function in electron-stimulated AES can be found from analysis of the experimental AES spectrum over an energy range of several hundred electron-volts.[38–40]

Guided by these results, we now divide the surface into two depth regions: the surface region, which is the outermost $5–10\lambda_i$ of the solid; and the subsurface region, which corresponds to depths $\gtrsim 5–10\lambda_i$. The results of this section regarding information on in-depth distribution of atoms contained in the detailed spectral peak shape can then be summarized as follows. Information on the atomic concentration–depth profile in the surface region up to depths $\sim 5\lambda_i$ is primarily determined by the spectral energy region up to ~ 100 eV below the peak energy and is essentially completely determined by the energy region up to ~ 200 eV below the peak. The spectral intensity for energies more than 200 eV below the peak energy has a significant contribution from electrons originally excited at depths larger than $5–10\lambda_i$.

Primary and secondary structural parameters

In the previous section we established the connection between the spectral energy range and the depth of origin of electrons that contribute to the spectrum. In this section we will estimate the number of structural parameters that can be determined from analysis of the spectrum.

The cross-section for electron energy loss in solids is in general a wide function of energy loss. There is therefore considerable overlap in the intensity contribution at a given spectral energy from electrons excited at different depths. This is the reason why there is not a direct one-to-one connection between depth of origin and energy loss (see previous section).

To estimate the amount of information that can be extracted from an energy spectrum, we first note that most solids have cross-sections that are at a maximum for 15–30 eV energy loss and that have a full width at half-maximum of 15–25 eV.[48] As a rule of thumb, each 15–30 eV of the spectrum therefore gives information from which one structural parameter can be determined. For example, the intensity and shape of the spectrum in the energy range up to ~ 100 eV from the peak is primarily determined by three and essentially completely determined by six structural parameters. We therefore divide the structural parameters that describe the chemical composition of the outermost $5–10\lambda_i$ of the solid into two groups: *primary* and *secondary* parameters.

The primary parameters are the three most important parameters needed to describe the main characteristics of the distribution of atoms within depths up to $5–10\lambda_i$. Two of these parameters describe the structure and the third gives the number of atoms within the structure. The two parameters that characterize the structure are not sufficient to determine the number of atoms because the structure may contain several types of atoms and their concentration may vary. For example, the three primary parameters for a rectangular structure are the start and end depths and the concentration of analysed atoms within that depth range. Likewise, for an island structure, the three primary parameters are the surface coverage, the island height and the concentration of analysed atoms within the island.

The secondary parameters are additional parameters in excess of the three primary parameters that characterize the finer details of the depth distribution of atoms in the outermost $5–10\lambda_i$ of the surface region. Normally there will be only three secondary parameters because more than six parameters that characterize the structure of this depth range can seldom be determined with any degree of accuracy from analysis of the energy spectrum. The spectrum does, however, contain information on more than six structural parameters if the spectrum is analyzed over an energy range considerably larger than 100 eV. The extra parameters describe the structure of the deeper layers ($>5–10\lambda_i$) because it is primarily electrons excited at these larger depths that determine the shape of the spectrum beyond ~ 100 eV from the peak energy (see previous section). So analysis of a larger energy range than 100 eV does not add much to the information on the details of the structure in the outermost $5\lambda_i$ but gives the possibility to determine additional structural parameters that describe the structure for larger depths.

EXPERIMENTAL STUDIES

In the foregoing sections it was argued that the level of accuracy of quantification in surface analysis cannot be

found without specifying in more detail what is quantified. This is related to the surface sensitivity of the techniques applied in quantitative surface analysis. From analysis of theoretical model spectra we then formulated specific objectives of quantification, namely two regions of depths (i.e. the outermost 5–10λ_i and larger depths) and two sets of parameters (the primary and secondary parameters) to define the concentration–depth profile of the outermost 5–10λ_i.

In this section we shall find the level of accuracy in quantification of these parameters. We will base this investigation on analysis of three experiments. We have chosen here three of the first experiments where peak shape analysis was applied.[19,20,28] Since then, several other experimental systems have been studied with the technique,[19–41] but the three early experiments serve well to study the uncertainty in the quantification. In addition, the present work will also give a new and improved analysis of these experiments because the previous analysis was based on less accurate algorithms than in the present analysis. Here we use a formalism that takes into account multiple electron scattering and we use a software package that allows a wide variety of in-depth distributions to be studied and provides a simpler and more direct quantification procedure.[18] This results in a more detailed, accurate and complete analysis of these three experiments in comparison to the previously published analysis.[19,20,28]

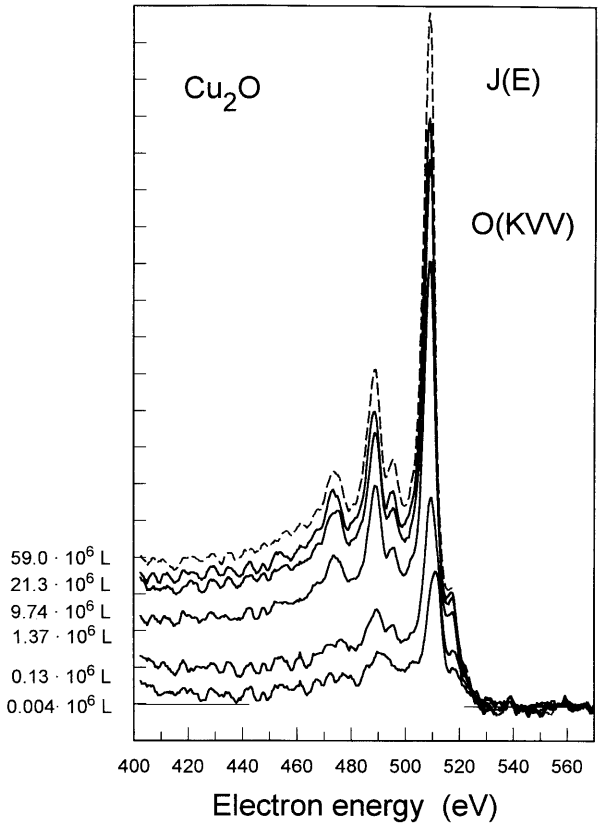

Figure 5. Oxygen KVV Auger spectra from a copper sample after different oxygen exposures. The Auger transition is excited with Mg Kα radiation.

Copper oxide growth on copper

This system was studied in Ref. 19. The copper foil was exposed *in situ* to oxygen at 2×10^{-3} Torr while being held at 650°C. This combination of temperature and oxygen pressure lies in the range where only Cu_2O and no CuO is formed.[70] That no CuO was formed was also checked after each exposure to oxygen by analysis of the Cu 2p spectrum.[19]

The O 1s peak overlaps in energy with the Cu LMM Auger peak. When peaks from two different atoms overlap in energy, the peak shape analysis technique is more involved. This is because $F(E)$ is different for the two atoms. Therefore, the spectra for each of the two atoms must be calculated separately and then added before it is compared to the measured spectrum. Rather than using the O 1s peak in the analysis of this particular system, it was therefore more convenient to apply the O KVV Auger peak excited with Mg Kα radiation.

Figure 5 shows O KVV Auger spectra measured for different oxygen exposures. The exposures are given in Table 1 and the curves in Fig. 5 show spectra corresponding to six of these oxygen exposures. The spectra were obtained by subtracting from the measured O KVV spectra the spectrum from pure copper in the same energy range after normalizing to the intensity level in the background on the high energy side of the O KVV peak. This procedure was found necessary for the lowest two exposures where the O KVV signal is quite small. For the remaining seven exposures there was no difference in the analysis between this procedure and the usual procedure, where a straight line is fitted on the high energy side of the O KVV peak region and then subtracted from the entire spectrum.

All spectra had first been corrected for the energy dependence of the analyser transmission, which was

Table 1. Structures of grown Cu_2O determined from analysis of O KVV (Figs 5–8)

Oxygen exposure (L)[a]	Coverage	Island Height	Total amount of Cu_2O (Å)
$\sim 4 \times 10^3$	0.28 ± 5%	25 ± 20%	7 ± 15%
0.129×10^6	0.34 ± 5%	60 ± 20%	20 ± 15%
0.804×10^6	0.60 ± 5%	90 ± 30%	54 ± 20%
1.37×10^6	0.66 ± 5%	Height > 100 Å ($\sim 5\lambda_i$)	
4.07×10^6	0.78 ± 3%	Height > 100 Å ($\sim 5\lambda_i$)	
9.74×10^6	0.82 ± 3%	Height > 100 Å ($\sim 5\lambda_i$)	
21.3×10^6	0.88 ± 2%	Height > 100 Å ($\sim 5\lambda_i$)	
42.9×10^6	0.93 ± 2%	Height > 100 Å ($\sim 5\lambda_i$)	
59.0×10^6	1.00	∞	

[a] 1 Langmuir = 10^{-6} Torr · s.

taken to be inversely proportional to the square root of the electron energy. The spectra have been smoothed by an 11-point Savitzky–Golay smooth with second-degree polynomial fit. This is not essential for the analysis procedure and the only reason for this smoothing is that when, as here, multiple colours are not used in figures it is simply impossible on a plot to distinguish two noisy spectra that are close together.

Now the peak shape analysis formalism is applied to these spectra; $\lambda_i = 19.0$ Å is used as estimated from the Seah and Dench formula.[13] The sample corresponding to the highest exposure is assumed to have oxygen with constant concentration to all relevant depths (i.e. at least $\sim 10\lambda_i$). Then the optimum value of B in the Universal cross-section is found for this system by analysing the spectrum in Fig. 5 corresponding to 59×10^6 L exposure with an assumed profile that is homogeneous to all depths. The best value of B is the one that gives approximately zero intensity over a wide energy range below the peak. This results in $B = 2900$ eV^2 and the spectrum is the lowest one in Fig. 6. This spectrum is used as a reference $F(E)$ spectrum in all the following analysis. The spectra in Fig. 5 were analysed under variation of the primary parameters of the surface structure until the resulting spectrum in each case matches the reference $F(E)$ spectrum with respect to both absolute peak area and peak shape. It was found that a satisfactory analysis of the spectra can only be achieved when the Cu_2O is distributed in the form of islands (see below). The parameters are shown in Table 1 and the resulting $F(E)$ spectra are shown in Fig. 6.

The uncertainty on the structural parameters in Table 1 is now estimated. In Fig. 7, the spectrum corresponding to 0.129×10^6 L oxygen exposure is analyzed under the assumption that the small amount of Cu_2O is distributed as a uniform layer over the surface (i.e. coverage = 1.0). Figure 7 shows the analysis as the thickness d of the oxide layer is varied until it matches the reference spectrum. With $d = 7$ Å the peak intensity is matched, but the intensity further away from the peak is clearly wrong. With $d = 60$ Å, the intensity for energies far below the peak energy is zero, as it should be, but the peak intensity is wrong by a factor of three. It is therefore obvious that there is no solution with coverage = 1.0. The behaviour of $F(E)$ for a wide parameter range can easily be found and by comparison to the $F(E)$ reference the uncertainty in parameter values can readily be estimated. The resulting values are: coverage = 0.34 ± 5%; island height = 60 Å ± 20% (see Table 1 and Fig. 6).

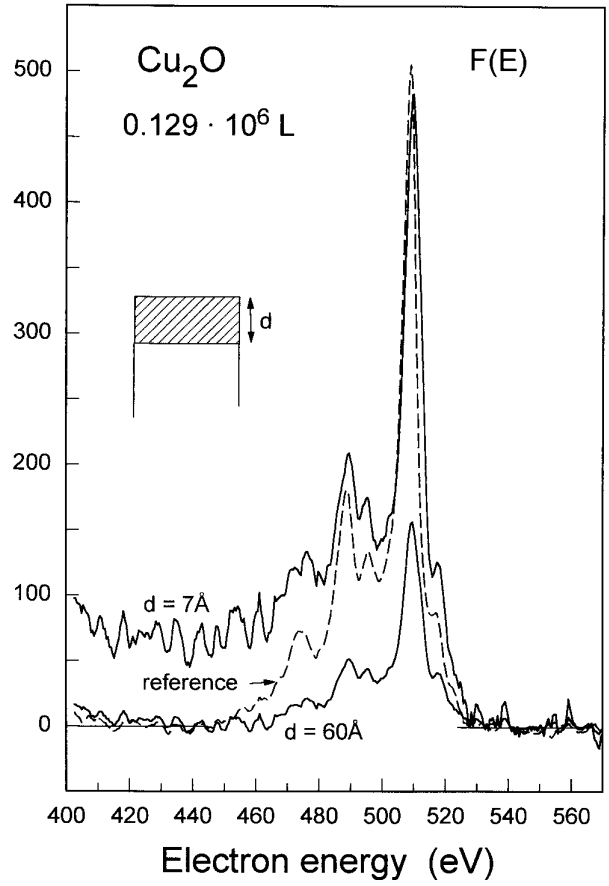

Figure 7. The spectrum of the sample exposed to 0.129×10^6 L oxygen (Fig. 5) after analysis, assuming that the oxide covers the complete surface. From this it is concluded that the oxide does not cover the complete surface.

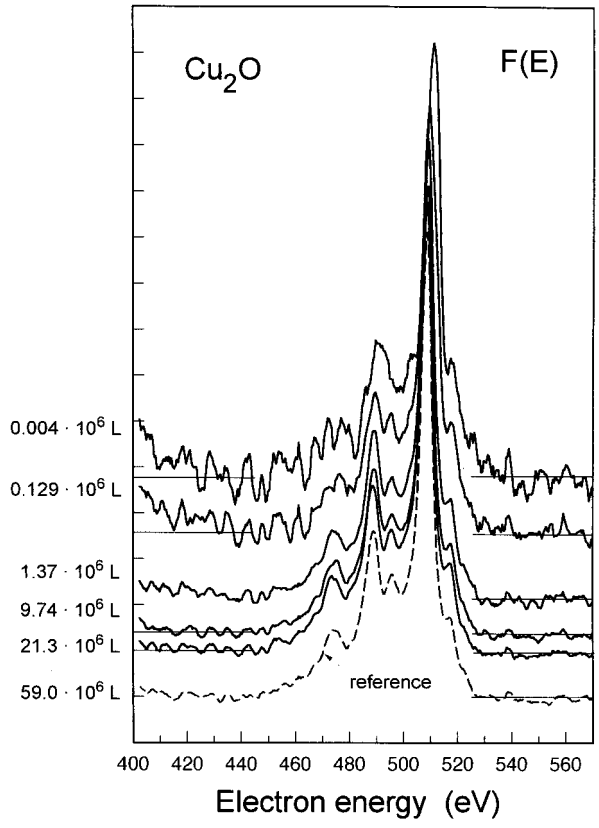

Figure 6. The spectra in Fig. 5 after analysis with the parameters given in Table 1.

As another example, the spectrum corresponding to 9.74×10^6 L oxygen exposure is analysed in Fig. 8. The optimum values, which are given in Table 1, are found by variation of the primary structural parameters (i.e. thickness and surface coverage of the copper oxide) and the resulting spectrum is shown in Fig. 6. Figure 8(a) illustrates that the agreement with the reference spectrum is significantly worse when the coverage is 0.72 and 0.92 rather than the optimum value of 0.82. Figure 8(b) shows that with 0.82 coverage, the island height must be at least 100 Å. After considering further sets of parameter values, the conclusion is quickly reached that

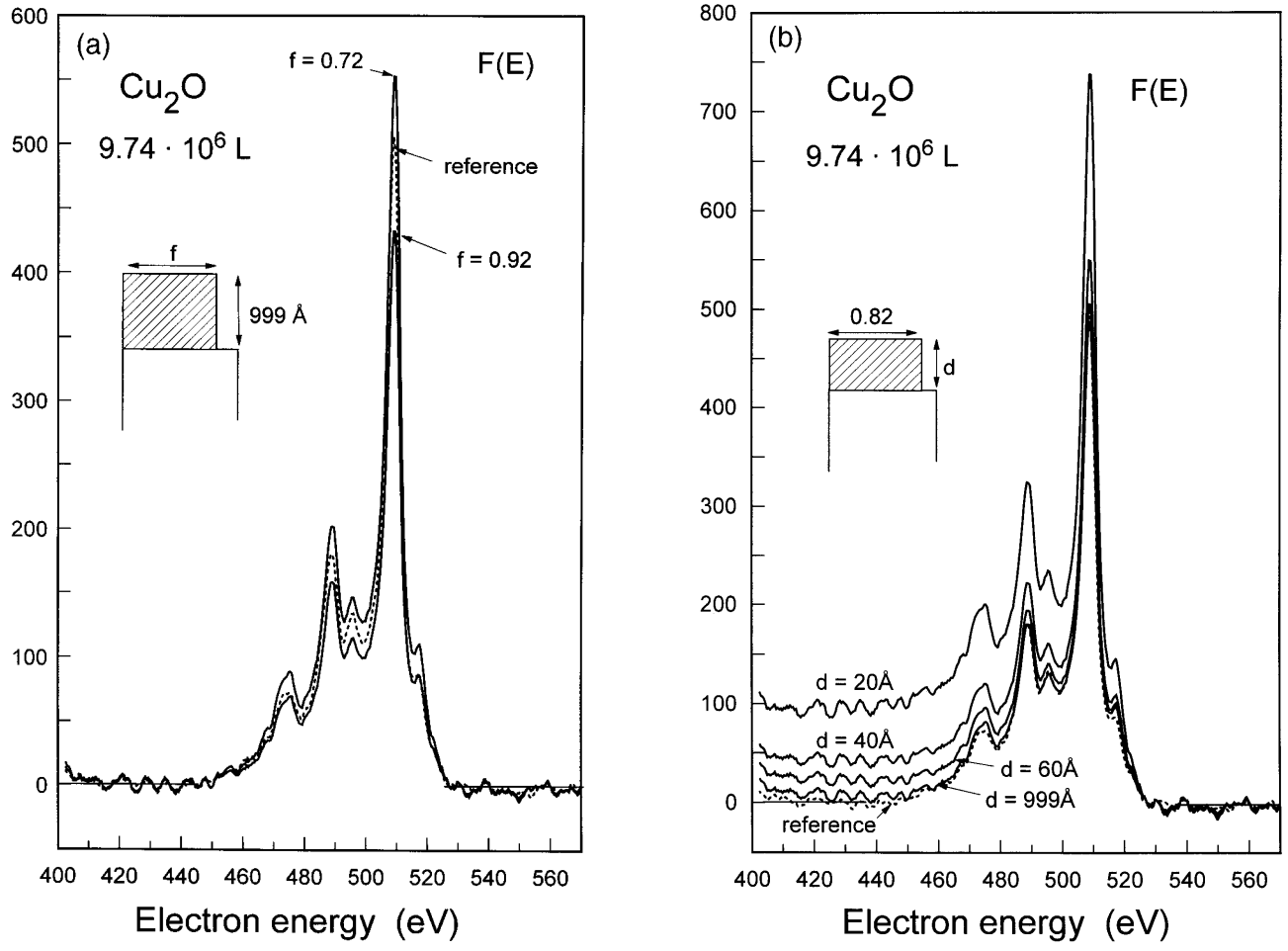

Figure 8. Analysis of the spectrum from the sample exposed to 9.74×10^6 L oxygen (Fig. 5). The analysis illustrates the sensitivity of the technique to variations in the parameters that define the structure of the copper oxide.

the Cu_2O thickness is larger than 100 Å and the Cu_2O islands cover a 0.82 ± 0.03 fraction of the surface. The determined structural parameters as well as their uncertainty are given in Table 1 for all exposures.

From the determined parameters in Table 1 we can now conclude the following concerning the growth of Cu_2O. Initially the oxidation occurs at nucleation centres and Cu_2O grows into the interior of the solid and forms island structures. Simultaneously the islands grow laterally to cover an increasingly larger fraction of the surface. After $\sim 10^6$ L of oxygen exposure, islands of Cu_2O that extend at least 100 Å into the solid have been formed. Upon further oxygen exposure, the islands grow laterally and form larger islands that eventually coalesce to form a thick film of fully oxidized Cu_2O. These conclusions, which were readily found from analysis of the XPS spectra, are in general agreement with previous results based on scanning electron microscopy studies.[71,72]

Gold marker in Ni

Structures where a thin gold layer is buried at varying depths in a nickel sample were studied in Ref. 28. A sputter-cleaned and 850°C-annealed Ni single crystal was mounted in an ultrahigh vacuum (UHV) chamber with base pressure in the low 10^{-10} Torr range. A small amount of Au was evaporated onto the Ni(111) surface. This was followed by consecutive *in situ* Ni evaporations onto the surface of that same sample. All evaporations were done at room temperature. After each evaporation, a spectrum of the Au 4d region was recorded. The Al Kα radiation was at 60° to the surface normal and the Au 4d electrons were detected in a direction normal to the surface with a hemispherical analyser operated at a constant 150 eV pass energy. The spectra were corrected for the analyser transmission function, which was assumed to vary with energy E as $E^{-1/2}$. Finally a straight line was fitted to each spectrum on the high-energy side of the peak and this was subtracted from the spectrum.

Figure 9 shows the measured spectra after being exposed to a mild Savitzky–Golay smooth. The upper spectrum was taken after evaporation of a small, but unknown amount of Au onto the Ni(111) surface. The spectra with progressively smaller intensity were taken after each evaporation of small and unknown amounts of Ni on top of this structure. Because of the way the samples were produced, the amount of gold in each of the five samples is exactly the same. Moreover, one would expect the gold to be present as a thin layer buried at increasing depths in the five samples. However, in practical surface analysis of a given sample nothing is known about the surface composition. Rather, the purpose of quantitative surface analysis is to determine the sample composition within the surface

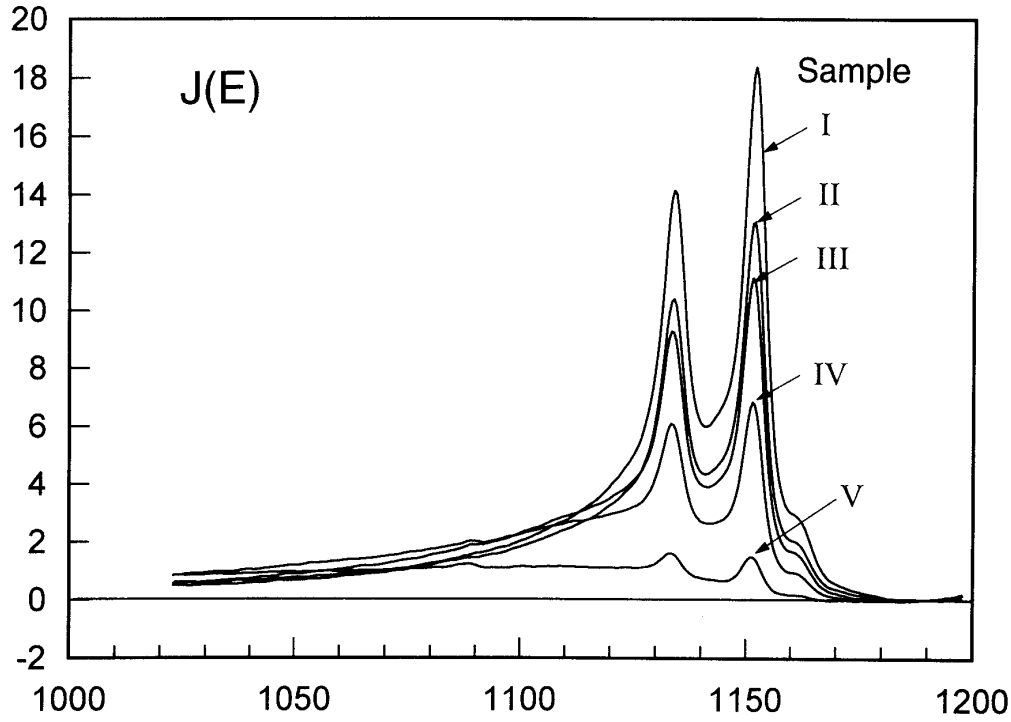

Figure 9. Gold 4d spectra measured from a thin gold layer on top of a nickel surface (I) after evaporations of different amounts of nickel on top (II–V).

region based on analysis of the measured spectrum. We shall therefore analyse the spectra separately without making any assumptions about the actual in-depth composition.

In contrast to the analysis of the Cu_2O system, the analysis is done here without use of a reference spectrum from a pure Au sample. This results in an uncertainty of $\sim$10% in the analysis of the reference spectrum. When a reference spectrum from a pure metal is used, this uncertainty is absent because both the depth profile and the concentration are known for a pure metal. However, the uncertainty in parameters determined below is independent of which reference spectrum is used. This 10% uncertainty in the analysis of the reference spectrum is therefore given in parentheses in Table 2.

The reference spectrum is found by analysis of spectrum I, using $\lambda_i = 14.2$ Å for 1150 eV electrons in Au.[11] Analysis of the other spectra (II–V) were done with $\lambda_i = 16.38$ Å for 1150 eV electrons in Ni[11].

Figure 10 illustrates the procedure used for analysis of spectrum IV. The analysis is done with three structures: an overlayer, a substrate and a buried layer model. In each case, the parameters that define the three structures are varied to give the same peak intensity in the analysed spectrum as in the reference spectrum. The overlayer and substrate models give extremely bad agreement, while a buried layer extending from 15.0 Å to 26.8 Å gives good agreement with both peak intensity and the peak shape of the reference spectrum. In this way the structures of each of the samples were determined. In each case, a buried layer distribution gave the best fit to the reference spectrum. The resulting spectra are shown in Fig. 11 and the determined start and end points for the layer are listed in Table 2. In all cases, there is an almost perfect agreement with both peak intensity and peak shape of the reference spectrum (see Fig. 11).

The uncertainty in the determined parameter values is also given in Table 2. It is determined by varying each parameter until a clearly worse visual agreement with the reference spectrum results.

We will now determine the sensitivity of the analysis to variations in the basic model structure of the depth profile. To this end, we now analyse the spectra with a model that consists of two narrow profiles of atoms, each corresponding to the number of atoms in a width δX, placed at varying depths $X_0 \pm DX$ centred around

Table 2. Structures of a set of Ni/Au/Ni samples determined from analysis of Au 4d (Figs 9–12)

Sample	Model: Buried layer		Two deltas at max. separation			Deviation
	$X_1 - X_2$	ΔX	X_0	DX	$2\delta X$	$(\Delta X - 2\delta X)/\Delta X$
I	0 − 14.5(±10%)	14.5(±10%)	7.25	6	13.5	6.9%
II	4.3 − 16.0 ± 10%	11.7 ± 3%	10.15	6	11.0	6.0%
III	7.5 − 19.8 ± 10%	12.3 ± 5%	13.65	6	11.6	5.7%
IV	15 − 26.8 ± 5%	11.8 ± 5%	20.9	6	11.1	5.9%
V	37 − 46 ± 5%	8.8 ± 10%	41.5	8	8.4	6.7%
RMS scatter		15.5%			16.6%	

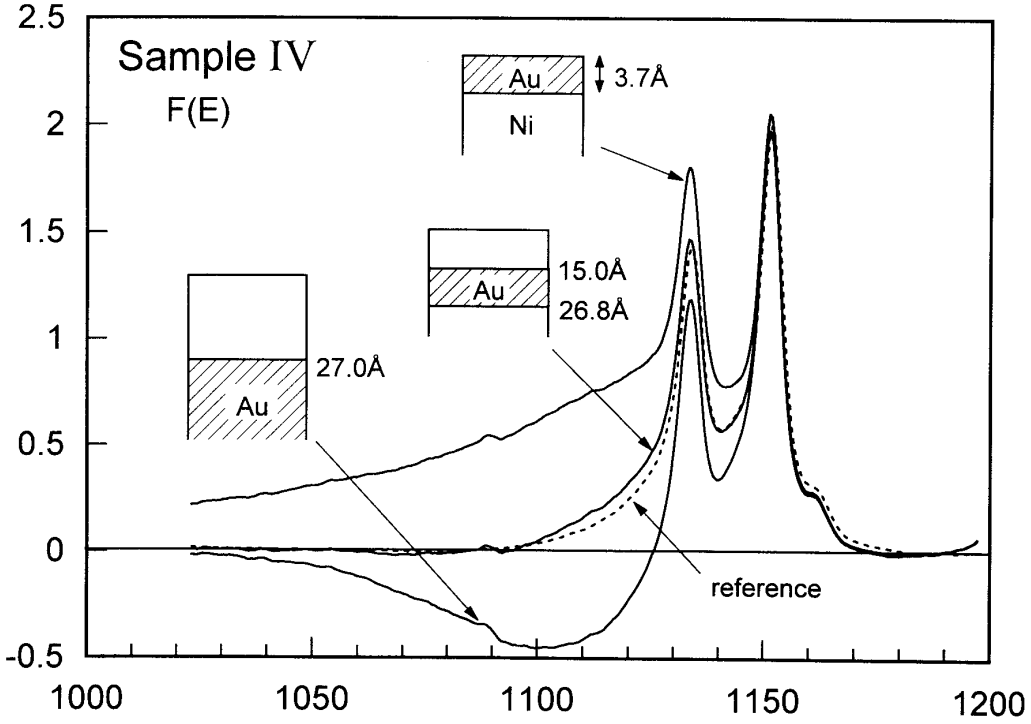

Figure 10. Analysis of the spectrum from sample IV (Fig. 9). The analysis illustrates how it can be concluded unambiguously that the gold in this sample is present as a buried layer.

the mean depth X_0 determined from the analysis with a buried layer (see Fig. 12). To determine the uncertainty in the determined structure, the distance DX was varied until a clearly worse visual agreement with the reference spectrum resulted. For each DX, δX was varied to give the best agreement with the reference spectrum. The determined maximum value of DX is 6 Å, except for the sample with the largest amount of nickel overlayer, for which the maximum DX is 8 Å (see Table 2). This means that the uncertainty in the model structure is ~ 6 Å, which, with $\lambda_i = 16.38$ Å, corresponds to $\sim 0.35\lambda_i$.

The quantitative amount of gold ($2\delta x$) determined with this model structure is also shown in Table 2. It varies only by 6% in comparison to the total amount (ΔX) determined when using the buried layer model. The uncertainty in quantification of the total amount of

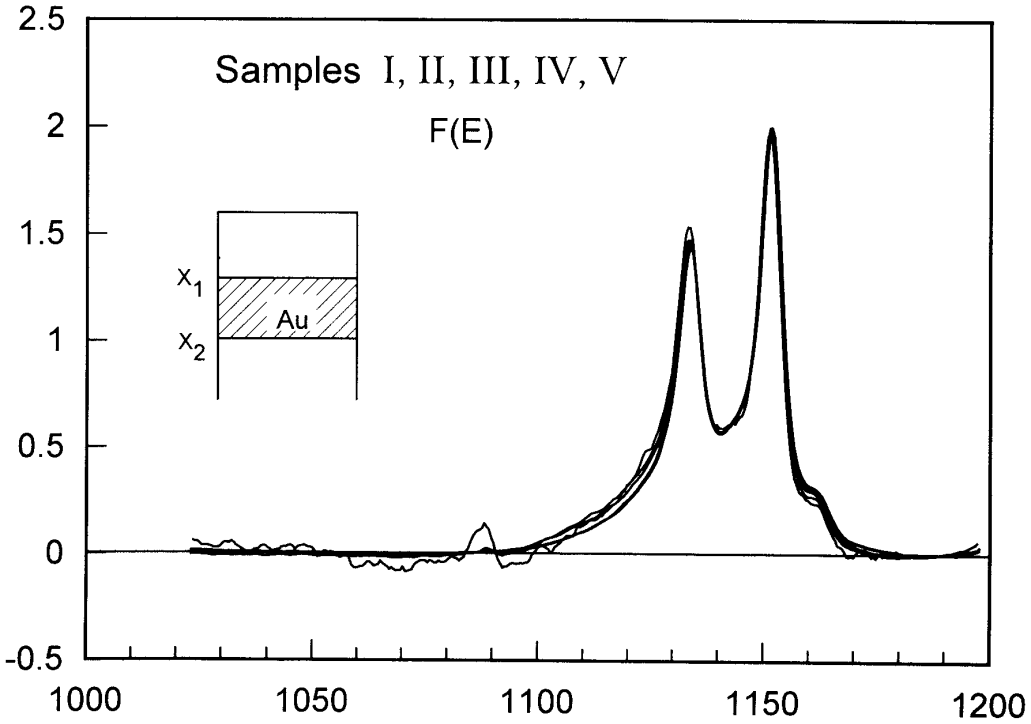

Figure 11. Determination of the nanostructures of samples II–V from analysis of their spectra (Fig. 9). The determined structural parameters are given in Table 2.

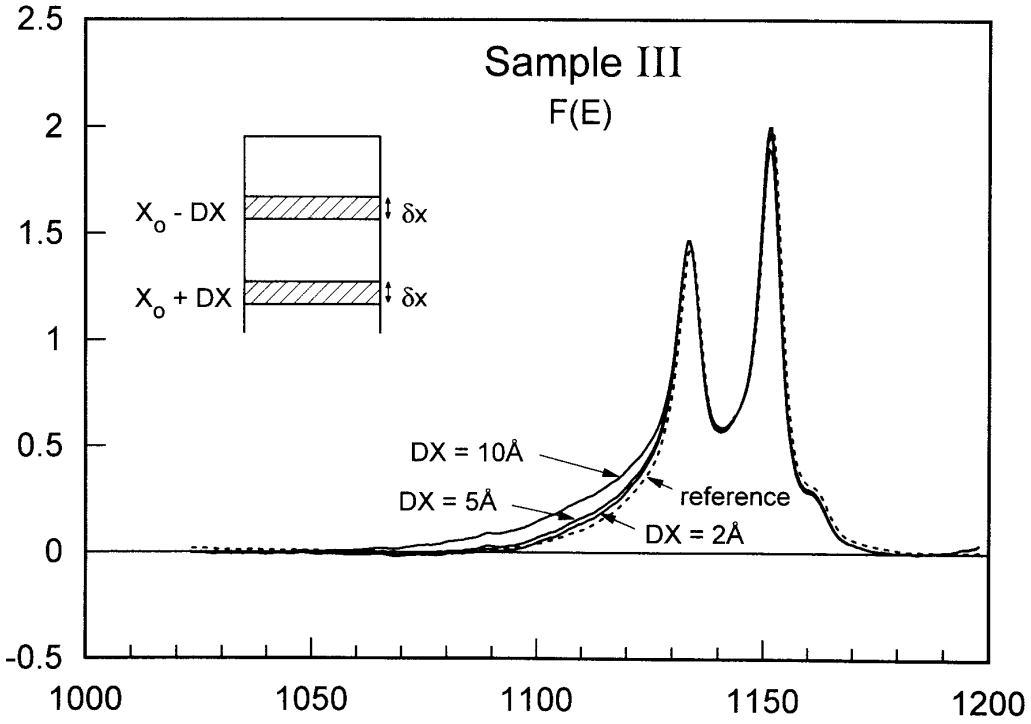

Figure 12. Analysis of the spectrum from sample III (Fig. 9) under the assumption that the gold is present as two thin layers. The purpose of this analysis is to study the sensitivity of the technique to variations in the model structure (see results in Table 2 and the text).

atoms is thus considerably smaller than the uncertainty in the structural parameters that define the in-depth distribution. This reflects the general property of the technique: that the parameters that describe the surface structure are correlated in such a way that the quantification of the total amount of atoms within the surface region is always considerably less uncertain than the individual structural parameters.

The five samples contain exactly the same number of gold atoms within the surface region. Therefore, the error on the absolute quantification can be estimated by comparing the total width ΔX determined for the five samples. The root-mean-square (RMS) scatter around the mean value is 15.4% (see Table 2). When the effects of elastic scattering of the electrons is approximated by Eqn (3), the ΔX values are changed as shown in Table 3.[57] The scatter is now smaller with an overall RMS value of 11%.

The conclusion of the analysis in this section (see Table 2) is that:

(1) The model structure is determined with a depth resolution of $\sim \pm \lambda_i/3$.

Table 3. Thickness ΔX of the determined layer (in Table 2) when elastic scattering effects are approximated by Eqn (3)

Sample	ΔX
I	13.4
II	11.2
III	12.2
IV	13.4
V	15.4
RMS scatter	11%

(2) The uncertainty in quantification of the primary structural parameters is better than $\pm 10\%$.

(3) The absolute quantification for solids with widely different surface structures shows an RMS scatter of $\sim 15\%$.

Ytterbium growth on Ni(100)

The growth of Yb on Ni(100) was studied in Ref. 20. The experiments were carried out in a UHV system with base pressure below 10^{-10} Torr. The surface was sputter-cleaned and annealed at 800°C until surface contamination was below the 1% level and sharp LEED spots were observed. High-purity Yb was evaporated onto the Ni(100) surface from a hot tungsten filament. X-ray photoelectron spectroscopy of the energy regions corresponding to the Ni 2p and Yb 4d peaks was carried out using Mg Kα radiation and a hemispherical electron energy analyser positioned at 15° to the surface normal. Subsequently, the sample was annealed for 6 min at 400°C and XPS spectra of Ni 2p and Yb 4d were recorded again. Reference spectra were also taken of the pure nickel sample prior to evaporation and of a sample produced by evaporating a thick Yb layer onto the Ni surface. All spectra were corrected for the analyser transmission function, which was assumed to vary with energy E as $E^{-1/2}$. Finally a straight line was fitted to each spectrum on the high-energy side of the peak and subtracted from the entire spectrum. Figure 13 shows the measured spectra. The spectra were analysed using the inelastic mean free paths $\lambda_{Ni} = 9.1$ Å and $\lambda_{Yb} = 19.0$ Å[11] for the Ni 2p and Yb 4d spectra, respectively. The optimum value of B in the Universal cross-section was found by analysing the spectra corresponding to pure Ni and thick Yb with a rectangular depth profile extending to infinite depths.

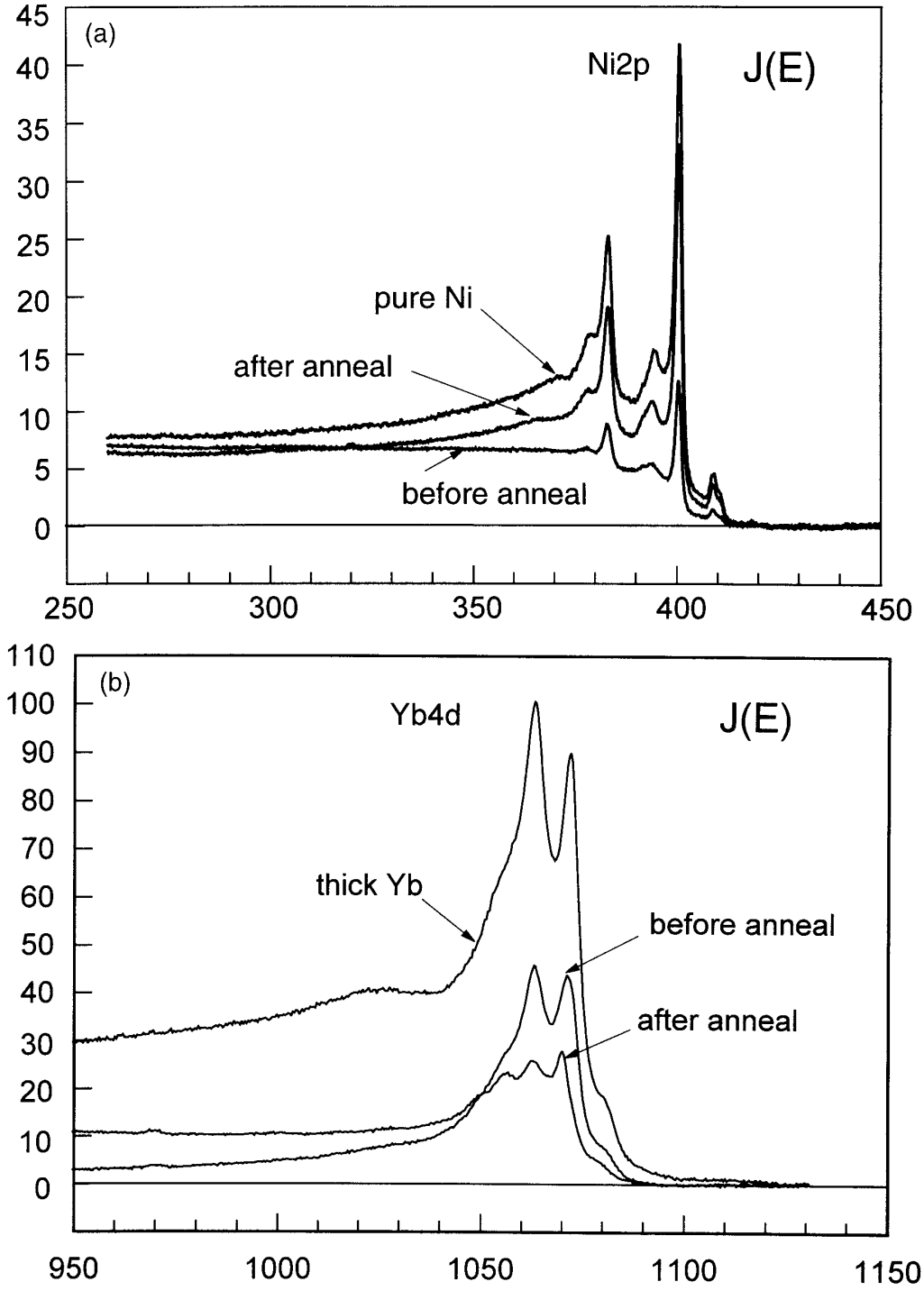

Figure 13. The Ni 2p and Yb 4d spectra of a Ni solid with evaporated Yb on top. Also shown are the spectra after the solid was annealed and a spectrum from a pure Ni and Yb solid.

The best value of B is the one that gives approximately zero intensity over a wide range below the peak. This results in $B_{\mathrm{Ni\ 2p}} = 3000\ \mathrm{eV}^2$ and $B_{\mathrm{Yb\ 4d}} = 2950\ \mathrm{eV}^2$ and the primary spectra are shown in Fig. 14. These spectra are used as reference $F(E)$ spectra in the following analysis.

Then the other four spectra were analysed under variation of the primary and secondary parameters of the surface structure until the resulting spectrum in each case matches the reference $F(E)$ spectrum with respect to both absolute intensity and peak shape.

Before annealing. In analysis of the Ni 2p spectrum before annealing [Fig. 13(a)] we first consider a depth distribution described only by the three primary structural parameters. The structure that gives the best agreement of the analysed Ni 2p spectrum with the reference is a substrate covered with an overlayer of 11 Å height covering 0.93 of the surface (see Table 4).

When we consider structures that also involve secondary parameters, an equally good agreement with the Ni 2p reference spectrum is obtained with a structure that consists of two islands [see Fig. 14(a)]: one with

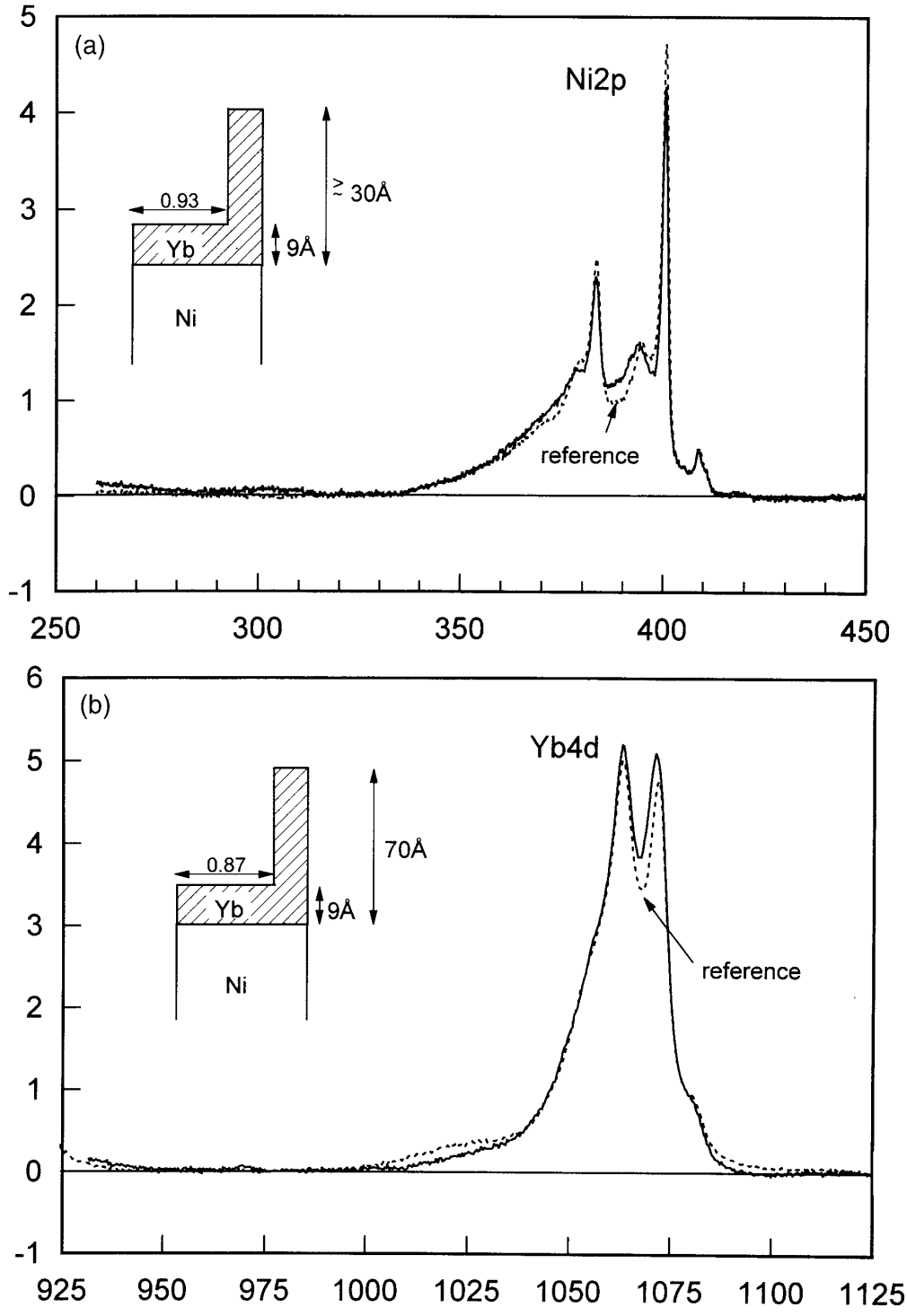

Figure 14. Determination of the structure of the Ni/Yb sample from analysis of the Ni 2p (a) and Yb 4d (b) spectra. The determined structural parameters are given in Table 4.

coverage 0.93 and height 9 Å and the other with coverage 0.07 and height $\gtrsim$30 Å. (The latter means that one cannot see clear differences in the spectra when this island height exceeds 30 Å. This depth corresponds to $\sim 3\lambda_{\mathrm{Ni}\,2\mathrm{p}}$. The depth probed then seems smaller than the $5\text{–}10\lambda_{\mathrm{i}}$ found above. The reason for this is that the majority of the influence on peak shape in this structure comes from the other island that covers a 0.93 fraction of the surface and only a minor spectral contribution originates from the influence of the island that covers only a 0.07 fraction of the surface.)

For analysis of the Yb 4d spectrum before annealing [Fig. 13(b)], the best agreement of the analysed Yb 4d peak with the Yb 4d reference is obtained with a two-island model corresponding to Stranski–Krastanov growth [see Fig. 14(b)]. A single-island model gave a worse agreement for all possible parameters. The best single-island parameter values were obtained with coverage 0.77 and island height 17.8 Å and this gave an analysis that was slightly worse than the best structure. These values are therefore given in parentheses in Table 4.

Table 4. Structures of a set of Ni/Au/Ni samples determined from analysis of Au 4d (Figs 9–12)

	Island 1		Island 2		
Sample	Coverage	Height (Å)	Coverage	Height (Å)	Total amount of Yb (Å)
Before annealing					
Ni 2p	0.93 ± 5%	11 ± 5%	–	–	10.2 ± 5%
Ni 2p	0.93 ± 5%	9 ± 10%	0.07	$\gtrsim$30	~10.5
Yb 4d	0.87 ± 10%	9 ± 10%	0.16 ± 30%	55 ± 35%	14.7 ± 5%
Yb 4d	(0.77%)	(17.8)	–	–	(13.7)
After annealing					
Ni 2p	0.75 ± 2%	Height > 100 Å (~10λ)	Thickness of possible second island cannot exceed 0.3 Å (~0.03λ_i)		
Yb 4d	0.29 ± 3%	Height > 120 Å (~6λ)	Thickness of possible second island cannot exceed 0.4 Å (~0.02λ_i)		

Although the two structures determined from analysis of the Ni 2p and Au 4d spectra are almost the same, there are slight differences in the absolute parameter values. This may be ascribed to the uncertainty in the applied values for λ_i. Thus with $\lambda_{Ni\,2p} = 9.5$ Å a satisfactory agreement of the Ni 2p spectrum with the reference is obtained with the same structural parameters as found from analysis of the Yb 4d peak.

After annealing. Analysis of both Ni 2p and Yb 4d spectra after anneal (Fig. 13) gives best agreement with the reference spectra when Ni and Yb are both assumed to be distributed homogeneously to all depths (see Fig. 15 and Table 4). The Yb 4d peak from the annealed sample reveals a pronounced new structure, which shows that Yb has reacted chemically with Ni and formed an alloy. The conclusion then is that after annealing Yb and Ni have formed a homogeneous alloy in the surface region.

The detailed analysis shows that Ni and Yb atoms in this homogeneous alloy extend at least 100 Å and 120 Å, respectively, into the solid (see Table 4). This corresponds to the depths $10\lambda_i$ and $6\lambda_i$ for the two peaks. Including secondary parameters in the analysis shows that if we assume a Stranski–Krastanov structure where one layer of atoms covers the total surface, the thickness of this layer must be smaller than 0.3 Å and 0.4 Å, respectively (see Table 4). Because this is smaller than one monolayer of atoms, we can exclude the Stranski–Krastanov structure for the sample after annealing.

The determined concentrations of Ni and Yb are relative to the concentrations of pure Ni and Yb. To find the composition of the alloy, differences in atomic densities must be corrected. We denote the Ni concentration in the alloy relative to the concentration in pure nickel by X^0_{Ni} and get, for the composition of the alloy

$$\frac{X_{Ni}}{X_{Yb}} = \frac{X^0_{Ni}\, a^3_{Yb}}{X^0_{Yb}\, a^3_{Ni}} \tag{14}$$

where for atom A

$$a_A{}^3 = \frac{W_A}{N\rho_A} \times 10^{21}$$

where a_A is in nm, $N = 6.02 \times 10^{23}$ is Avogadro's number, W_A is the atomic weight and ρ_A is the density (in g cm^{-3}) of solid A. This gives $a^3_{Ni} = 0.0110$ nm^3 and $a^3_{Yb} = 0.0412$ nm^3. The atomic densities in pure Ni and Yb thus differ by more than a factor of two. With $X^0_{Ni} = 0.75$ and $X^0_{Yb} = 0.29$ found here (see Table 4) and with $X^0_{Ni} + X^0_{Yb} = 1$, this yields (with Eqn (14)) $X_{Ni} = 0.91$ and $X_{Yb} = 0.09$, i.e. the approximate alloy composition is $Ni_{0.9}\,Yb_{0.1}$.

SUMMARY AND CONCLUSIONS

The accuracy of XPS and AES quantification by peak shape analysis has been studied here from a detailed analysis of a range of model spectra and three sets of experiments. The results can be summarized as follows.

Information on the concentration–depth profile in the surface region up to ~5λ_i depth is primarily contained in the spectral energy region up to ~100 eV below the peak energy and is essentially completely contained by the energy region up to ~200 eV below the peak. The spectral intensity for energies more than 200 eV below the peak energy depends only slightly on the depth distribution of atoms at depths smaller than ~2–3λ_i and has a significant contribution from electrons originally excited at depths larger than 5–10λ_i. The depth probed by the technique varies with the actual depth distribution of the sample being analysed and, as expected, the method is more sensitive to the atomic distribution at large depths if the atomic concentration at shallow depths is small. The maximum depth probed by analysis of a spectrum in a range ~100 eV below the peak energy is thus typically 5λ_i but it may be as high as 10λ_i.

We divided the structural parameters that describe the chemical composition of the outermost 5–10λ_i of the solid into two groups: primary and secondary parameters. The primary parameters are the three most important parameters needed to describe the main characteristics of the distribution of atoms within depths up to 5–10λ_i. The secondary parameters are parameters, in excess of the three primary parameters, that characterize the finer details of the depth distribution of atoms in the outermost 5–10λ_i of the surface region. Normally there will be only three secondary parameters because more than six parameters that characterize the structure of this depth range can seldom be determined with any degree of accuracy from analysis of the energy spectrum.

Analysis of a larger energy range than 100 eV does not add much to the information on the details of the structure in the outermost 5λ_i but gives the possibility

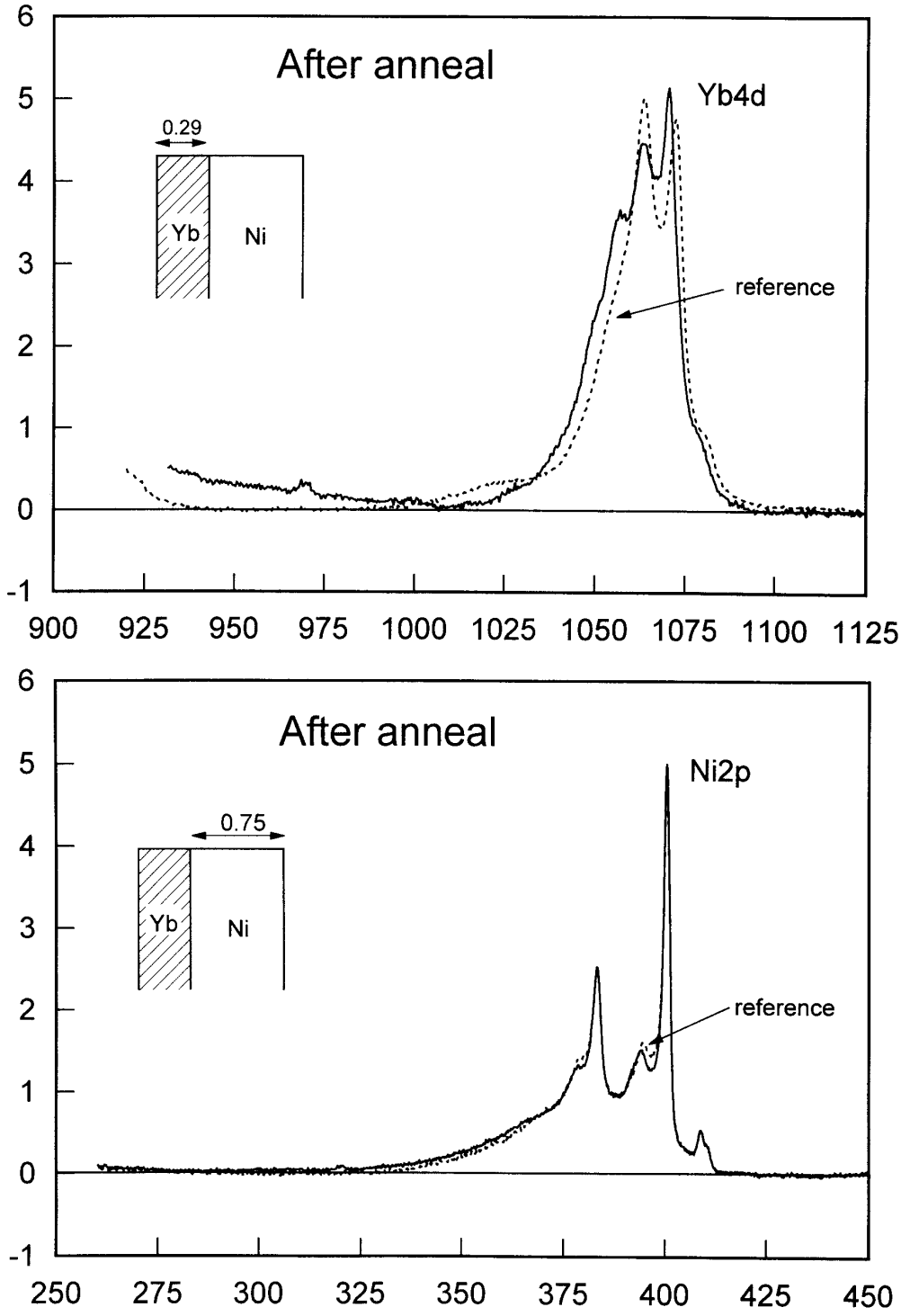

Figure 15. Determination of the structure of the annealed Ni/Yb sample from analysis of the Ni 2p (a) and Yb 4d (b) spectra. The determined structural parameters are given in Table 4.

to determine additional structural parameters that describe the structure for larger depths.

The uncertainty in the determined three primary parameters is typically 5–10% but may vary from ~2% to ~20%. The highest values of ~20% are found for noisy spectra. The lowest values ~2% are found for spectra where the signal strength is high and where there is no chemically induced changes in peak shape. The latter implies that the shape of a reference spectrum can be applied in the detailed comparison of peak shapes also in the near-peak region. This gives a stronger constraint and thereby a more certain determination of the structural parameters.

The uncertainty in the determined secondary parameters is higher and amounts typically to $\gtrsim 35\%$.

The depth resolution is $\sim 1/3\lambda_i$ in the sense that two distinctly different models of depth profiles can be distinguished when the two models vary significantly over a depth of more than $\sim 1/3\lambda_i$ at any depth $< 5\lambda_i$.

The uncertainty in the total determined amount of atoms within the surface region is ~5–10% as long as the depths are within the primary probing depth of the

method (i.e. $<5\lambda_i$). This uncertainty in the quantification is significantly less than the uncertainty in the individual parameters that describe the structure. This is so because the structural parameters are correlated, i.e. the analysis procedure will force one parameter to change if another is changed in such a way that the quantitative amount of atoms changes only little with changes in any one of the assumed structural parameters.

The absolute quantification of a set of samples where the in-depth distribution varies considerably gives an RMS scatter of 15%.

Table 5 gives a summary of the most important results.

Table 5. Accuracy in quantification of the outermost $\sim 5\lambda_i$ depth

Quantity	Total amount of material	Three primary parameters	Three secondary parameters	Depth resolution for primary parameters
Uncertainty	~5–10%	5–10%	$\gtrsim$35%	$\sim 0.35\lambda_i$

REFERENCES

1. M. P. Seah, in *Practical Surface Analysis*, Vol. 1, ed. by D. Briggs and M. P. Seah, Chapt. 5. Wiley, New York (1990).
2. C. J. Powell and M. P. Seah, *J. Vac. Sci. Technol. A* **8**, 735 (1990).
3. C. J. Powell, *Surf. Interface Anal.* **11**, 103 (1988).
4. M. P. Seah, *Surf. Interface Anal.* **9**, 85 (1986).
5. M. P. Seah, *Surf. Interface Anal.* **20**, 243 (1993).
6. A. Jablonski, *Surf. Interface Anal.* **15**, 559 (1990).
7. S. Tougaard and P. Sigmund, *Phys. Rev. B* **25**, 4452 (1982).
8. S. Tougaard, *Surf. Interface Anal.* **11**, 453 (1988).
9. S. Tougaard, *J. Electron Spectrosc.* **52**, 243 (1990).
10. S. Tougaard and C. Jansson, *Surf. Interface Anal.* **20**, 1013 (1993).
11. S. Tanuma, C. J. Powell and D. R. Penn, *Surf. Interface Anal.* **11**, 577 (1988).
12. S. Tanuma, C. J. Powell and D. R. Penn, *J. Electron Spectrosc.* **62**, 95 (1993).
13. M. P. Seah and W. A. Dench, *Surf. Interface Anal.* **1**, 2 (1979).
14. S. Tougaard, *J. Vac. Sci. Technol. A* **14**, 1415 (1996).
15. C. R. Brundle, C. A. Evans and S. Wilson (eds), *Encyclopedia of Materials Characterization, Surfaces, Interfaces and Thin Films*. Butterworth-Heinemann, London (1992).
16. S. Tougaard and H. S. Hansen, *Surf. Interface Anal.* **14**, 730 (1989).
17. S. Tougaard, *Appl. Surf. Sci.* **100**, 1 (1996).
18. S. Tougaard, *QUASES: Software Package for Quantitative XPS/AES of Surface Nano-Structures by Peak Shape Analysis*, Version 2.0 (1997). (Contact S. Tougaard for more information.)
19. S. Tougaard, W. Hetterich, A. H. Nielsen and H. S. Hansen, *Vacuum* **41**, 1583 (1990).
20. S. Tougaard and H. S. Hansen, *Surf. Sci.* **236**, 271 (1990).
21. T. Ogama and T. Horikawa, *J. Vac. Sci. Technol. A* **8**, 2204 (1990).
22. M. Repoux, *Surf. Interface Anal.* **18**, 567 (1992).
23. Zeggane and M. Delamar, *Appl. Surf. Sci.* **29**, 411 (1987).
24. H. Tokutaka, N. Ishihara, K. Nishimori, S. Kishida and K. Isomoto, *Surf. Interface Anal.* **18**, 697 (1992).
25. J. Végh, *Surf. Interface Anal.* **18**, 545 (1992).
26. K. H. Richter, *J. Electron Spectrosc.* **60**, 127 (1992).
27. L.-S. Johansson and T. Losoi, *Surf. Interface Anal.* **17**, 230 (1991).
28. S. Tougaard, H. S. Hansen and M. Neumann, *Surf. Sci.* **244**, 125 (1991).
29. H. S. Hansen, S. Tougaard and H. Biebuyck, *J. Electron Spectrosc.* **58**, 141 (1992).
30. M. Sastry, *Surf. Interface Anal.* **20**, 815 (1993).
31. M. Sastry, S. Pal, D. V. Paranjape and P. Ganguly, *J. Electron Spectrosc. Relat. Phenom.* **67**, 163 (1994).
32. M. Schleberger, D. Fujita, C. Scharfschwerdt and S. Tougaard, *Surf. Sci.* **331–333**, 942 (1995).
33. H. S. Hansen, C. Jansson and S. Tougaard, *J. Vac. Sci. Technol. A* **10**, 2938 (1992).
34. M. Schleberger, D. Fujita, C. Scharfschwerdt and S. Tougaard, *J. Vac. Sci. Technol. B* **13**, 949 (1995).
35. D. Fujita, M. Schleberger and S. Tougaard, *Surf. Sci.* **331–333**, 343 (1995).
36. B. S. Norgren, M. A. J. Somers and J. H. de Wit, *Surf. Interface Anal.* **21**, 378 (1994).
37. A. Jouaiti, A. Mosser, M. Romeo and S. Shindo, *J. Electron Spectrosc.* **59**, 327 (1992).
38. D. Fujita, M. Schleberger and S. Tougaard, *Surf. Interface Anal.* **24**, 211 (1996).
39. D. Fujita, M. Schleberger and S. Tougaard, *Surf. Sci.* **357/358**, 180 (1996).
40. M. Schleberger, D. Fujita and S. Tougaard, *Electron Spectrosc. Relat. Phenom.* **82**, 173 (1996).
41. M. Schleberger, A. C. Simonsen, S. Tougaard, J. L. Hansen and A. Nylandsted Larsen, *J. Vac. Sci. Technol. A* **15**, 3032 (1997).
42. J. W. Gadzuk, *J. Electron Spectrosc.* **11**, 355 (1977).
43. W. Gadzuk, in *Photoemission and the Electronic Properties of Surfaces*, ed. by B. Feuerbacher, B. Fitton and R. F. Willis, p. 111. Wiley, New York (1978).
44. D. Chastenet and P. Longe, *Phys. Rev. Lett.* **44**, 91 (1980).
45. S. Bose, P. Kiehm and P. Longe, *Phys. Rev. B* **23**, 712 (1981).
46. G. K. Mårtensson and A. Nielsson, *J. Electron Spectrosc. Relat. Phenom.* **52**, 1 (1990).
47. S. Tougaard, *Solid State Commun.* **61**, 547 (1987).
48. S. Tougaard, *Surf. Interface Anal.* **25**, 137 (1997).
49. Doniach and Sunjic, *J. Phys. C* **3**, 285 (1970).
50. P. M. van Attekum and G. K. Wertheim, *Phys. Rev. Lett.* **43**, 1896 (1979).
51. D. R. Penn, *Phys. Rev. Lett.* **40**, 568 (1978).
52. S. Tougaard, *Phys. Rev. B* **34**, 6779 (1986).
53. C. P. Lund, S. M. Thurgate and A. B. Wedding, *Phys. Rev. B* **49**, 11357 (1994).
54. C. S. Fadley, in *Synchrotron Radiation Research: Advances in Surface Science*, ed. by R. Z. Bachrach. Plenum Press, New York (1990).
55. W. F. Egelhoff, Jr., in *Ultrathin Magnetic Structures I; An Introduction to Electronic, Magnetic and Structural Properties*, ed. by J. A. C. Bland and B. Heinrich. Springer, Berlin (1994).
56. A. Jablonski and S. Tougaard, *Surf. Interface Anal.* **22**, 129 (1994); *NIST Elastic-Electron-Scattering Cross-Section Database*, Standard Reference Data Program, Database 64. National Institute of Standards and Technology, Gaithersburg (1996).
57. S. Tougaard and A. Jablonski, *Surf. Interface Anal.* **25**, 404 (1997).
58. S. Tougaard and A. Jablonski, *Surf. Interface Anal.* **23**, 559 (1995).
59. W. S. M. Werner, W. H. Gries and H. Störi, *Surf. Interface Anal.* **17**, 693 (1991).
60. I. S. Tilinin and W. S. Werner, *Phys. Rev.* **46**, 13739 (1992).
61. V. M. Dwyer and J. M. Richards, *Surf. Interface Anal.* **18**, 555 (1992).

62. P. J. Cumpson and M. P. Seah, *Surf. Interface Anal.* **25**, 430 (1997).
63. A. Jablonski and S. Tougaard, *Surf. Interface Anal.* **26**, 17 (1998).
64. A. Jablonski and S. Tougaard, *Surf. Interface Anal*, to be published.
65. J. Osterwalder, T. Greber, S. Hüfner, H. A. Aebischer and L. Schlapbach, in *The Structure of Surfaces III*, ed. by S. Y. Tong, M. A. van Hove, K. Takayanagi and X. D. Xie, p. 91. Springer-Verlag, Berlin (1991).
66. C. Scharfschwerdt, J. Kutscher, F. Schneider, M. Neumann and S. Tougaard, *J. Electron Spectrosc.* **60**, 321 (1992).
67. S. Y. Tong, H. C. Poon and D. R. Snider, *Phys. Rev. B* **32**, 2096 (1985).
68. H. E. Bishop, *Surf. Interface Anal.* **16**, 118 (1990).
69. P. Alnot, J. Olivier and C. S. Fadley, *J. Electron Spectrosc.* **49**, 159 (1989).
70. R. D. Smidt-Whitney, M. Martinez-Clemente and A. Revcolevschi, *J. Cryst. Growth* **23**, 113 (1974).
71. K. Heinemann, D. Bhogeswara Rao and D. L. Douglass, *Oxid. Met.* **9**, 379 (1975).
72. G. G. Hembree, J. M. Cowley and M. A. Otooni, *Oxid. Met.* **13**, 331 (1979).

